

Ultrathin Films of Superconducting Metals as a Platform for Topological Superconductivity

Chao Lei,¹ Hua Chen,^{2,3} and Allan H. MacDonald¹

¹*Department of Physics, The University of Texas at Austin, Austin, Texas 78712, USA**

²*Department of Physics, Colorado State University, Fort Collins, CO 80523, USA*

³*School of Advanced Materials Discovery, Colorado State University, Fort Collins, CO 80523, USA*

The ingredients normally required to achieve topological superconductivity (TSC) are Cooper pairing, broken inversion symmetry, and broken time-reversal symmetry. We present a theoretical exploration of the possibility of using ultra-thin films of superconducting metals as a platform for TSC. Because they necessarily break inversion symmetry when prepared on a substrate and have intrinsic Cooper pairing, they can be TSCs when time-reversal symmetry is broken by an external magnetic field. Using microscopic density functional theory calculations we show that for ultrathin Pb and β -Sn superconductors the position of the Fermi level can be tuned to quasi-2D band extrema energies using strain, and that the g -factors of these Bloch states can be extremely large, enhancing the influence of external magnetic fields.

Introduction—Topological superconductors (TSC)[1–6] can host fault-tolerant qubit operations based on the exchange properties[7, 8] of Majorana zero modes located either at the ends of topological superconducting quantum wires[9], or in the vortex cores of two-dimensional TSCs[1, 3, 7, 10]. For weak Cooper pairing, topological superconductivity occurs whenever the host normal metal has an odd number of closed Fermi surfaces. TSCs were first realized[11–14] some years ago by combining[15, 16] low density-of-states semiconductors, with strong spin-orbit coupling and external magnetic fields that lift band spin-degeneracies, and Cooper pairing provided by an adjacent superconductor. In recent research semiconductor-based TSCs have been further refined[17, 18], and other possibilities have also been realized experimentally, including the TSCs based on magnetic atomic chains on superconducting substrates[19–21] and two-dimensional (2D) TSCs based on topological insulator surface states[22, 23].

TSC has been proposed as a theoretical possibility in bulk superconductors that might have chiral order parameters [24–33], for example in noncentrosymmetric superconductors[29, 30, 33] with broken time-reversal or inversion symmetry. These intrinsic systems, including SrTiO₃/LaAlO₃ heterostructures [24–26, 28], bulk Sr₂RuO₄, and superfluid He³, have some potential advantages over the artificial hybrid materials systems in which TSC has already been achieved experimentally. There is however no intrinsic system in which all the ingredients required for TSC states are fully established. In the case of SrTiO₃/LaAlO₃ heterostructures, for example, it seems difficult to achieve a sufficiently large Zeeman coupling strength since the g -factor in SrTiO₃/LaAlO₃ is small [34], much smaller than in Majorana platforms based on semiconductor quantum wires which have large g -factors up to 20-50[13, 17, 18].

In this article we propose a different possibility, namely establishing 2D TSC directly in ultrathin films of superconducting metals [35], instead of semiconductors,

thereby avoiding problems associated with establishing proximity coupling between a semiconductor and a superconductor. We are motivated by recent experimental demonstrations of strong robust superconductivity in ultra-thin metal films [36–38], and by proposals for realizing topological superconductivity based on strong Rashba-like spin-orbit interactions in the surface-states of heavy metals TSC[39, 40]. We show that quasi 2D band extrema in ultra-thin superconducting films can occur close to the Fermi level, that in the cases of Pb and β -Sn films the g -factors at the relevant band edges can be extremely large, and that band positions can be tuned by strain. We predict that these ingredients will allow thin superconducting films to be tuned to TSC states when time-reversal invariance is broken by a weak magnetic field or a proximitized exchange interaction[38].

We concentrate below on lead (Pb) and β -Sn thin films. Using *ab initio* density functional theory (DFT) calculations [41], we show that the strength of inversion symmetry breaking in β -Sn and Pb thin films can be controlled by varying either film thickness or substrate material, that Fermi level positions relative to band extrema are more easily tuned by strain than by gate electric fields, and that typical g -factors[42] at band extrema are extremely large. Strains can be varied experimentally by placing the thin film on a piezoelectric substrate as illustrated in Fig. 1, and adjusted to tune in topologically non-trivial states.

Superconducting metal thin film as TSCs — For weak pairing TSC occurs in bands that are effectively spinless when an odd number of them cross the Fermi energy. In quasi-2D systems with strongly broken inversion symmetry, Rashba-like spin-orbit interactions lift spin-degeneracies except at the time-reversal invariant \mathbf{k} points where Kramers theorem applies. The Kramers degeneracy can be lifted only by breaking time-reversal invariance, for example by an external magnetic field. A minimal mean field theory shows that, like the current semiconductor systems, these TSCs are class D

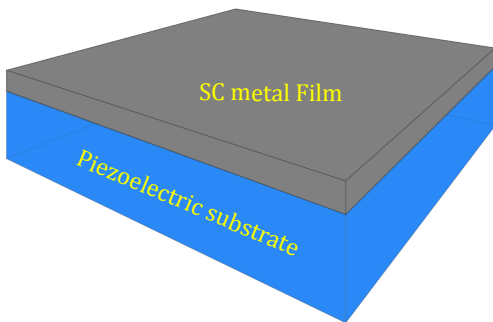


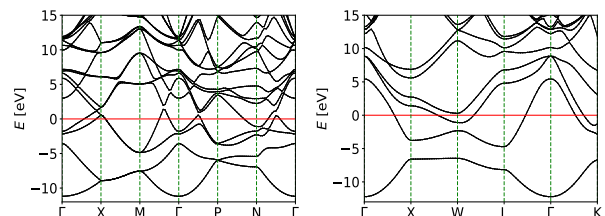
FIG. 1: Schematic illustration of an ultra-thin heavy superconducting(SC) metal film grown on a piezoelectric substrate. An electric field applied to the substrate can then be used to tune the film into a topological superconducting state.

according to the Altland-Zirnbauer (AZ) classification [41, 43] which is also the main class of systems (1D or 2D) studied in present experiments. For sufficiently strong spin-orbit coupling a TSC state is realized when $\Delta_z = g\mu_B B > \sqrt{\Delta^2 + \mu^2}$, where Δ_z is the Zeeman energy, Δ is the pair potential, and μ is the chemical potential measured from the zero-field band energy at the time-reversal invariant \mathbf{k} -point. Topological superconductivity in quasi-2D systems therefore requires that μ be small and that the g -factor that describes the Kramers degeneracy splitting be large. A quasi-2D metal film has the advantage over its bulk counterpart that it has a greater density of bands, which increases the chances for large g -factors and is essential, as we shall see, if we want to find materials with small value of μ . Comparing the criteria that support large g -factors [44, 45] with patterns in the occurrence of superconductivity[46] suggests ultra-thin films of β -Sn and Pb as promising candidates for topological superconductivity.

TABLE I: Calculated g -factors at the Γ point for the band closest to the Fermi level in bulk and in thin films of β -Sn and Pb on a As_2O_3 substrate.[41, 42] For the films the average values of the g -factors of 12 subbands around Fermi level is also given. The g -factors are obtained by evaluating the splitting between a Kramers pair at the Γ point under a magnetic field. For the thin films the magnetic field is along the film normals [(111) for Pb and (001) for β -Sn], while for bulk Pb and β -Sn it is along the z -axis [(001) direction].

β -Sn	g -factor	avg.	Pb	g -factor	avg.
bulk	681		bulk	132	
7 layers	29	254	5 layers	57	140
9 layers	572	243	7 layers	161	73
11 layers	574	268	9 layers	198	186

Pb has a face-centered-cubic structure [41] and is a



(a) Bandstructure of β -Sn (b) Bandstructure of Pb

FIG. 2: Bandstructure of bulk β -Sn and Pb. The red horizontal lines mark the Fermi level. These bands are consistent with literature results for β -Sn [51, 52] and Pb [53]. Thin film quasi-2D bands can be crudely estimated from these bulk bands by discretizing the surface-normal momentum component.

widely studied superconductor with a bulk $T_c = 7.19$ K. Among the several stable phases of bulk Sn only β -Sn, which has a tetragonal structure (A5)[41], is a superconductor[47] with $T_c = 3.72$ K. The bands of β -Sn and Pb, illustrated in Fig. 2, reflect strong $s - p$ hybridization. Bulk β -Sn and bulk Pb both have inversion symmetry, and therefore even degeneracies of all bands throughout the Brillouin zone.

We evaluated g -factors using methods informed by recent advances in the *ab initio* description of orbital magnetism [42, 48–50]. According to our calculations[42], the Γ point g -factors of bulk β -Sn and bulk Pb are very large, as summarized in Table I. In Fig. 2 we see that a strongly dispersive band crosses the Fermi energy along Γ -X in β -Sn and along Γ -L in Pb. Based on this observation, we expect that quasi-2D subband extrema at energies close to the Fermi energy will occur at 2D Γ points in thin films with surface normals along the (111) direction and the (001) direction for Pb and β -Sn respectively. Indeed, it is (111) growth direction Pb films that are commonly studied experimentally. [36].

In thin films the inversion symmetry of a bulk structure does not survive for all surface terminations and thicknesses, even when the film structure consists of bulk unit cells repeated in the film normal direction. For β -Sn films grown along the (001) direction, inversion symmetry is absent when the number of atomic layers is odd[54]. As an illustration, the band structure of single layer Sn (001) is shown in Fig. 3a. The band closest to the Fermi level, which has its extremum near Γ , exhibits typical Rashba spin-orbit coupling behavior as illustrated in Fig. 3c. Similar quasi-2D bands are present for all odd-layer-number β -Sn (001) thin films[41]. The Rashba spin-orbit coupling strength becomes smaller with increasing number of layers. However, even at 15 layers, its value is still about 0.85 eV \AA , which is several times larger than that in semiconductor quantum wires ($\sim 0.2 \text{ eV \AA}$ [13]).

For Pb (111), on the other hand, inversion symmetry is maintained at all film thicknesses and every subband has

two-fold degeneracy throughout the 2D Brillouin zone. Fig. 3b shows the example of a two-layer Pb (111) thin film (see [41] for more band structures for different number of layers). Broken inversion symmetry must then come from hybridization with a substrate. In the calculations described below we have used a single quintuple layer of As_2O_3 with the Bi_2Te_3 structure as the substrate because it is insulating and, according to our DFT calculations, lattice-matched to Pb (111). The resulting quasi-2D band structure is illustrated in Fig. 3d (results for other thicknesses can be found in [41]). We can see in the figure that the extremum of the lowest band at Γ exhibits Rashba spin splitting. The Rashba spin-orbit coupling of Pb thin films on As_2O_3 is 0.15-0.4 eVÅ on average (0.01, 0.2, 0.34, and 0.05 eVÅ respectively for the four subbands around Fermi level [41]), which is much larger than that on Si substrates [55, 56] (0.03-0.04 eV Å for 10 layers of Pb). The averaged Rashba spin-orbit coupling decreases with increasing film thickness, but even for the thicker films considered here it is still large compared with that in semiconductor quantum wires on s-wave superconductors [13].

We also studied heavier substrates in the Pnictogen Chalcogenides family such as As_2O_3 , Sb_2S_3 , Sb_2Se_3 , Bi_2Se_3 , Bi_2Te_3 , and found an enhancement of Rashba spin-orbit coupling ranging from 0.3 eVÅ to around 0.7 eVÅ on average [41], and even larger for certain subbands. However, since some of Pnictogen Chalcogenides are topological insulators, those subbands may also be the surface states of topological insulators. For some Pb (111) thicknesses the band extremum closest to the Fermi level lies not at a time-reversal invariant momentum, but at the K -point where spin-splitting is present even in the absence of a magnetic field. In this case, valley symmetry breaking by an external magnetic field is necessary to yield a topological superconducting state.

Tuning the Fermi Level — As illustrated in Figs. 3c and 3d, the scale of the spin-orbit splitting in the metal thin films of interest is a sizable fraction of an eV and comparable to quasi-2D band widths. TSC states will therefore occur whenever the Fermi level is within Δ_z of a band extremum energy. Here Δ_z refers either to spin-splitting at a time-reversal invariant momentum, or to energetic splitting between spin-orbit split states at time-reversal partner momenta. For g -factors ~ 100 , these energies are ~ 10 meV at the fields to which superconductivity typically survives. (The Bohr magneton is ~ 0.058 meV/T. In Pb (111) thin films, $H_{c\perp} = 1.56$ T for 5 monolayers and 0.63 T for 13 monolayers. In-plane critical fields are much larger: $H_{c\parallel} = 54.9$ T for 5 monolayers and 13.6 T for 13 monolayers [36]). It follows that TSC states should be realizable if the Fermi level can be tuned to within ~ 10 meV of quasi-2D band extrema, for large Rashba coupling, the most possible pairing of electrons has an intra-band form. Due to the very large $H_{c\parallel}$, the system may be driven by in-plane fields into an

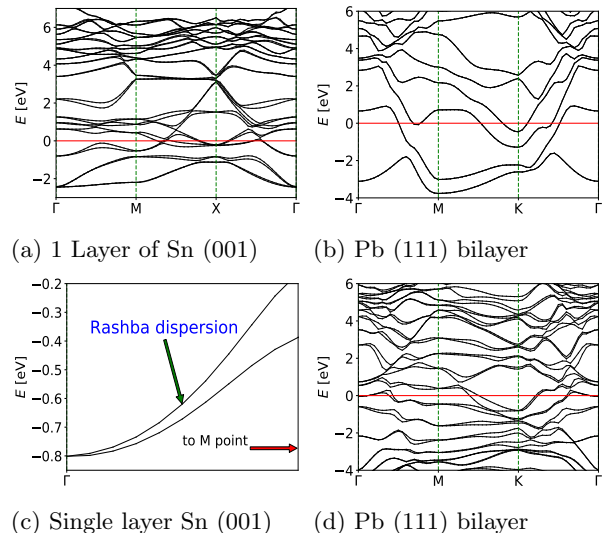


FIG. 3: Band structure of a single layer (3 atomic layers) film of β Sn grown along the (001) direction (a) and a Pb bilayer film grown along the (111) direction (b). (c) Highlight of the first band below the Fermi level in (a) near the Γ -point showing Rashba-like spin-orbit splitting. (d) Pb bilayer grown along the (111) direction on an As_2O_3 substrate exhibiting Rashba-like spin-orbit splitting near the Γ -point.

inter-band pairing phase with finite pairing momentum [57].

Figure 2 shows that bulk β -Sn bands cross the Fermi level along Γ -X, and that bulk Pb bands cross the Fermi level along Γ -L. The bandwidth of β -Sn from Γ to X is about $W = 2.765$ eV. It follows that the average distance between quasi-2D subband energies at any particular 2D \mathbf{k} -point is around $W/2N$, or ~ 150 meV for a 10 layer thick film. In Fig. 4a we plot the quasi-2D band energies at the Γ point measured from the Fermi level for odd-layer-number Sn thin films *vs.* the number of layers. As expected the energy separations tend to decrease with increasing film thickness, but are suitably small only occasionally. For the films with thickness of 7, 9 and 11 layers, band extrema are within tens of meV of the Fermi level. The calculated g -factors at the Γ point for these thicknesses are up to around 600. (The g -factors of the films highlighted by arrows in Fig. 4a are presented in Table I.) For bulk Pb the bandwidth from Γ to L is ~ 10 eV, implying larger typical energy separation values. The band separation plot for Pb (111) thin films is presented in Fig. 4b, which shows apparent quantum size effect oscillations due to confinement of electron wave functions along the thickness direction [58]. In spite of the larger typical separations, we find that at some thicknesses band extrema at Γ and K points can be within a few tens of meV of the Fermi level. Since the g -factors we calculated for Pb thin films, listed in Table I, are as large as ~ 200 ,

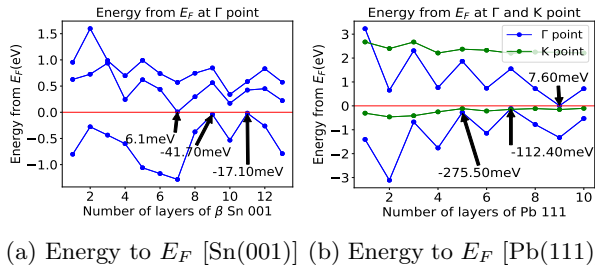


FIG. 4: (a) Subband energy extrema measured from E_F in β -Sn thin films grown in (001) direction. Small energy separations are highlighted by numerical values attached to arrows pointing to the position at which they are plotted. The smallest separation is 6.1 meV for a seven layer film. (b) Γ and K -point band extrema relative to the Fermi level for Pb (111) thin films.

topological superconductivity is still a possibility.

Because DFT is not likely to be perfectly predictive, and because energy separations are likely to be influenced by uncontrolled environmental effects, practical searches for TSC in metal thin films will be greatly assisted by *in situ* control. We have examined the efficacy of two possibilities. In Fig. 5a and 5b we show that, in spite of the strong screening effects expected in metals, external electric fields of ~ 1 V/nm in magnitude can still shift subband energy positions by ~ 10 meV for β -Sn (001) and by ~ 20 meV for Pb (111), which might be large enough to tune into topological states in some instances. The field scale of these calculations are however larger than what is typically practical. Assuming linear response a field of 10^{-1} V/nm [59] would typically change level separations by only ~ 1 meV. We have therefore also examined strain effects. In Figs. 5c and 5d, energy separations at the Γ point in β -Sn (001) and Pb (111) films are plotted *vs.* strain. The sensitivity of energy separation to a 1% strain is typically more than 50 meV for β -Sn (001) and around ~ 200 meV for Pb (111) (the case with a substrate is similar[41]), suggesting that strains in this range could successfully tune a thin film into a TSC state. Strains of this size can be induced electrically by applying an electric field across a piezoelectric substrate. If strain could be transferred from a substrate with a large piezoelectric effect ($1.6\text{nm}/\text{V}$)[60], an electric field of 10^{-2} V/nm could give a strain larger than 1%. We conclude that strain is more promising than direct external electric fields for tuning metal thin films into TSC states.

Discussion — Ultra-thin films of strongly spin-orbit-coupled superconducting metals have the advantage, compared to the commonly studied systems composed of semiconductors on superconducting substrates, that no interface or proximity effect is needed to achieve superconductivity in a strongly spin-orbit coupled system. We have shown that superconducting thin films with strong

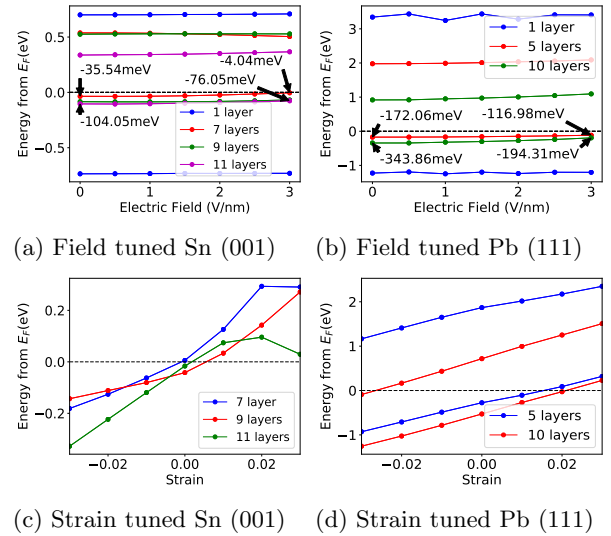


FIG. 5: Band extrema tuning via electric field and strain. (a) Γ -point band energy relative to the Fermi level as a function of electric field for a β -Sn (001) thin film. (b) Γ point band energy relative to the Fermi level as a function of electric field for a Pb (111) thin film. (c) Γ point band energy as a function of strain in the $\pm 3\%$ range for β -Sn (001) thin films. (d) Γ point band energy as a function of strain in the $\pm 3\%$ range for Pb (111) thin films.

spin-orbit coupling can be driven into a topological superconductor state by tuning with external electric fields or strains. We have evaluated g -factors[42] at the extrema of the quasi-2D bands of Pb and β -Sn, demonstrating that they have large values that limit the accuracy with which the band extrema energies need to be tuned to the Fermi level.

Ultra-thin film growth[61] is a key challenge that must be met to realize this proposal for topological superconductivity. Metal thin films growth is strongly influenced by quantum-size effects [61] that determine a discrete set of magic thicknesses at which smooth growth is possible. Further restrictions are imposed by the requirement that the film thickness not be too large[62] to allow strain tuning to be effectively employed. To our best knowledge single crystalline β -Sn thin film growth has not yet been achieved. Recent experiments have however already demonstrated superconductivity with strong spin-orbit coupling[36] in ultrathin films of Pb. Our results motivate experimental efforts to grow the β -Sn thin film and drive β -Sn and Pb thin film into TSC phase with a relatively weak magnetic field, or by depositing magnetic atoms or films.

Acknowledgements. — The authors thank Ken Shih for helpful discussions. This work was supported by the Office of Naval Research under grant ONR-N00014-14-1-0330 and the Welch Foundation under grant TBF1473.

The authors acknowledge the Texas Advanced Computing Center (TACC) at The University of Texas at Austin for providing HPC resources that have contributed to the research results reported within this paper.

* leichao.ph@gmail.com

- [1] C. Beenakker, *Annu. Rev. Con. Mat. Phys.* **4**, 113 (2013).
- [2] C. Beenakker and L. Kouwenhoven, *Nat. Phys.* **12**, 618 (2016).
- [3] A. Stern, *Nature* **464**, 187 (2010).
- [4] A. Jason, *Rep. Prog. Phys.* **75**, 076501 (2012).
- [5] L. Martin and F. Karsten, *Semicond. Sci. Technol.* **27**, 124003 (2012).
- [6] S. Masatoshi and A. Yoichi, *Rep. Prog. Phys.* **80**, 076501 (2017).
- [7] D. A. Ivanov, *Phys. Rev. Lett.* **86**, 268 (2001).
- [8] C. Nayak, S. H. Simon, A. Stern, M. Freedman, and S. Das Sarma, *Rev. Mod. Phys.* **80**, 1083 (2008).
- [9] A. Y. Kitaev, *Phys. Usp.* **44**, 131 (2001).
- [10] N. Read and D. Green, *Phys. Rev. B* **61**, 10267 (2000).
- [11] A. Das, Y. Ronen, Y. Most, Y. Oreg, M. Heiblum, and H. Shtrikman, *Nat. Phys.* **8**, 887 (2012).
- [12] M. T. Deng, C. L. Yu, G. Y. Huang, M. Larsson, P. Caroff, and H. Q. Xu, *Nano Lett.* **12**, 6414 (2012).
- [13] V. Mourik, K. Zuo, S. M. Frolov, S. R. Plissard, E. P. A. M. Bakkers, and L. P. Kouwenhoven, *Science* **336**, 1003 (2012).
- [14] L. P. Rokhinson, X. Liu, and J. K. Furdyna, *Nat. Phys.* **8**, 795 (2012).
- [15] R. M. Lutchyn, J. D. Sau, and S. Das Sarma, *Phys. Rev. Lett.* **105**, 077001 (2010).
- [16] J. D. Sau, R. M. Lutchyn, S. Tewari, and S. Das Sarma, *Phys. Rev. Lett.* **104**, 040502 (2010).
- [17] S. M. Albrecht, A. P. Higginbotham, M. Madsen, F. Kuemmeth, T. S. Jespersen, J. Nygrd, P. Krogstrup, and C. M. Marcus, *Nature* **531**, 206 (2016).
- [18] M. T. Deng, S. Vaitieknas, E. B. Hansen, J. Danon, M. Leijnse, K. Flensberg, J. Nygrd, P. Krogstrup, and C. M. Marcus, *Science* **354**, 1557 (2016).
- [19] S. Nadj-Perge, I. K. Drozdov, J. Li, H. Chen, S. Jeon, J. Seo, A. H. MacDonald, B. A. Bernevig, and A. Yazdani, *Science* **346**, 602 (2014).
- [20] B. E. Feldman, M. T. Randeria, J. Li, S. Jeon, Y. Xie, Z. Wang, I. K. Drozdov, B. Andrei Bernevig, and A. Yazdani, *Nat. Phys.* **13**, 286 (2016).
- [21] R. Pawlak, M. Kisiel, J. Klinovaja, T. Meier, S. Kawai, T. Glatzel, D. Loss, and E. Meyer, *npj Quantum Information* **2**, 16035 (2016).
- [22] Q. L. He, L. Pan, A. L. Stern, E. C. Burks, X. Che, G. Yin, J. Wang, B. Lian, Q. Zhou, E. S. Choi, K. Murata, X. Kou, Z. Chen, T. Nie, Q. Shao, Y. Fan, S.-C. Zhang, K. Liu, J. Xia, and K. L. Wang, *Science* **357**, 294 (2017).
- [23] Y. Zeng, C. Lei, G. Chaudhary, and A. H. MacDonald, *Phys. Rev. B* **97**, 081102 (2018).
- [24] N. Mohanta and A. Taraphder, *EPL (Europhysics Letters)* **108**, 60001 (2014).
- [25] M. S. Scheurer and J. Schmalian, *Nature communications* **6**, 6005 (2015).
- [26] F. Loder, A. P. Kampf, and T. Kopp, *Scientific reports* **5**, 15302 (2015).
- [27] T. Tzen Ong and P. Coleman, *Phys. Rev. B* **90**, 174506 (2014).
- [28] M. S. Scheurer, D. F. Agterberg, and J. Schmalian, *npj Quantum Materials* **2**, 9 (2017).
- [29] M. S. Scheurer, *Phys. Rev. B* **93**, 174509 (2016).
- [30] K. V. Samokhin, *Phys. Rev. B* **92**, 174517 (2015).
- [31] Y. Wang, G. Y. Cho, T. L. Hughes, and E. Fradkin, *Phys. Rev. B* **93**, 134512 (2016).
- [32] F. Loder, A. P. Kampf, T. Kopp, and D. Braak, *Phys. Rev. B* **96**, 024508 (2017).
- [33] N. Wennerdal and M. Eschrig, *Phys. Rev. B* **95**, 024513 (2017).
- [34] G. Cheng, M. Tomczyk, S. Lu, J. P. Veazey, M. Huang, P. Irvin, S. Ryu, H. Lee, C.-B. Eom, C. S. Hellberg, *et al.*, *Nature* **521**, 196 (2015).
- [35] C. Brun, T. Cren, and D. Roditchev, *Supercond. Sci. Technol* **30**, 013003 (2016).
- [36] H. Nam, H. Chen, T. Liu, J. Kim, C. Zhang, J. Yong, T. R. Lemberger, P. A. Kratz, J. R. Kirtley, K. Moler, P. W. Adams, A. H. MacDonald, and C.-K. Shih, *Proc. Natl. Acad. Sci. USA* **113**, 10513 (2016).
- [37] T. Zhang, P. Cheng, W.-J. Li, Y.-J. Sun, G. Wang, X.-G. Zhu, K. He, L. Wang, X. Ma, X. Chen, Y. Wang, Y. Liu, H.-Q. Lin, J.-F. Jia, and Q.-K. Xue, *Nature Physics* **6**, 104 (2010).
- [38] G. C. Menard, S. Guissart, C. Brun, R. T. Leriche, M. Trif, F. Debontridder, D. Demaille, D. Roditchev, P. Simon, and T. Cren, *Nat. Comm.* **8**, 2040 (2017).
- [39] A. C. Potter and P. A. Lee, *Phys. Rev. B* **85**, 094516 (2012).
- [40] L. Yan-Feng, W. Wen-Lin, Z. Yi-Min, D. Hao, L. Wei, W. Lili, H. Ke, S. Can-Li, M. Xu-Cun, and X. Qi-Kun, *Sci. Bull.* **62**, 852 (2017).
- [41] See Supplemental Material at [URL] for more information.
- [42] C. Lei, H. Chen, and A. H. MacDonald, to be published.
- [43] C.-K. Chiu, J. C. Y. Teo, A. P. Schnyder, and S. Ryu, *Rev. Mod. Phys.* **88**, 035005 (2016).
- [44] R. L. Hota, G. S. Tripathi, and J. N. Mohanty, *Phys. Rev. B* **47**, 9319 (1993).
- [45] R. Patnaik and G. Tripathi, *Solid State Commun.* **112**, 669 (1999).
- [46] M. Debessai, T. Matsuoka, J. J. Hamlin, W. Bi, Y. Meng, K. Shimizu, and J. S. Schilling, *J. Phys.: Confer. Series* **215**, 012034 (2010).
- [47] J. Eisenstein, *Rev. Mod. Phys.* **26**, 277 (1954).
- [48] G. P. Mikitik and Y. V. Sharlai, *Phys. Rev. B* **67**, 115114 (2003).
- [49] D. Xiao, J. Shi, and Q. Niu, *Phys. Rev. Lett.* **95**, 137204 (2005).
- [50] T. Thonhauser, D. Ceresoli, D. Vanderbilt, and R. Resta, *Phys. Rev. Lett.* **95**, 137205 (2005).
- [51] M. Miasek, *Phys. Rev.* **130**, 11 (1963).
- [52] J. E. Craven, *Phys. Rev.* **182**, 693 (1969).
- [53] A. D. Zdesis, E. N. Economou, and D. A. Papaconstantopoulos, *J. Phys. F* **10**, 1149 (1980).
- [54] M. E. Woods and B. J. Hopkins, *J. Phys. C* **18**, 217 (1985).
- [55] B. Slomski, G. Landolt, S. Muff, F. Meier, J. Osterwalder, and J. H. Dil, *New J. Phys.* **15**, 125031 (2013).
- [56] J. H. Dil, F. Meier, J. Lobo-Checa, L. Patthey, G. Bihlmayer, and J. Osterwalder, *Phys. Rev. Lett.* **101**, 266802 (2008).

- [57] L. Florian, P. K. Arno, and K. Thilo, *J. Phys. Condens. Matter* **25**, 362201 (2013).
- [58] C. M. Wei and M. Y. Chou, *Phys. Rev. B* **66**, 233408 (2002).
- [59] M. Oshiki and E. Fukada, *J. Mater. Sci.* **10**, 1 (1975).
- [60] D. E. Grupp and A. M. Goldman, *Science* **276**, 392 (1997).
- [61] Z. Zhang, Q. Niu, and C.-K. Shih, *Phys. Rev. Lett.* **80**, 5381 (1998).
- [62] M. Murakami and R. W. Vook, *Crit. Rev. Solid State Mater. Sci.* **11**, 317 (1983).
- [63] P. Giannozzi, S. Baroni, N. Bonini, M. Calandra, R. Car, C. Cavazzoni, D. Ceresoli, G. L. Chiarotti, M. Cococcioni, I. Dabo, A. Dal Corso, S. de Gironcoli, S. Fabris, G. Fratesi, R. Gebauer, U. Gerstmann, C. Gougoussis, A. Kokalj, M. Lazzeri, L. Martin-Samos, N. Marzari, F. Mauri, R. Mazzarello, S. Paolini, A. Pasquarello, L. Paulatto, C. Sbraccia, S. Scandolo, G. Sclauzero, A. P. Seitsonen, A. Smogunov, P. Umari, and R. M. Wentzcovitch, *J. Phys. Condens. Matter* **21**, 395502 (19pp) (2009).
- [64] P. Giannozzi, O. Andreussi, T. Brumme, O. Bunau, M. B. Nardelli, M. Calandra, R. Car, C. Cavazzoni, D. Ceresoli, M. Cococcioni, N. Colonna, I. Carnimeo, A. D. Corso, S. de Gironcoli, P. Delugas, R. A. D. Jr, A. Ferretti, A. Floris, G. Fratesi, G. Fugallo, R. Gebauer, U. Gerstmann, F. Giustino, T. Gorni, J. Jia, M. Kawamura, H.-Y. Ko, A. Kokalj, E. Kkbenli, M. Lazzeri, M. Marsili, N. Marzari, F. Mauri, N. L. Nguyen, H.-V. Nguyen, A. O. de-la Roza, L. Paulatto, S. Ponc, D. Rocca, R. Sabatini, B. Santra, M. Schlipf, A. P. Seitsonen, A. Smogunov, I. Timrov, T. Thonhauser, P. Umari, N. Vast, X. Wu, and S. Baroni, *J. Phys. Condens. Matter* **29**, 465901 (2017).
- [65] A. Dal Corso, *Comput. Mater. Sci* **95**, 337 (2014).
- [66] G. Kresse and J. Hafner, *Phys. Rev. B* **47**, 558 (1993).
- [67] G. Kresse and J. Hafner, *Phys. Rev. B* **49**, 14251 (1994).
- [68] G. Kresse and J. Furthmüller, *Comput. Mater. Sci* **6**, 15 (1996).
- [69] G. Kresse and J. Furthmüller, *Phys. Rev. B* **54**, 11169 (1996).
- [70] J. P. Perdew, K. Burke, and M. Ernzerhof, *Phys. Rev. Lett.* **77**, 3865 (1996).
- [71] J. P. Perdew, K. Burke, and M. Ernzerhof, *Phys. Rev. Lett.* **78**, 1396 (1997).
- [72] "Bismuth telluride (bi2te3) crystal structure, chemical bond, lattice parameters (including data for related compounds): Datasheet from landolt-brnstein - group iii condensed matter volume 41c: "non-tetrahedrally bonded elements and binary compounds i" in springermaterials,".
- [73] H. Zhang, C.-X. Liu, X.-L. Qi, X. Dai, Z. Fang, and S.-C. Zhang, *Nat. Phys.* **5**, 438 (2009).
- [74] K. Motizuki, H. Ido, T. Itoh, and M. Morifuji, (2009).
- [75] "Srtio3 crystal structure, lattice parameters: Datasheet from landolt-brnstein - group iii condensed matter volume 41e: "ternary compounds, organic semiconductors" in springermaterials,".

Supplementary Materials

Density functional theory calculations were performed using Quantum Espresso[63, 64] with PAW pseudopotentials[65] and the Vienna Ab initio simulation package (VASP)[66–69] with Generalized Gradient Approximation PBE[70, 71] pseudopotentials. The VASP software was used only for the calculations assessing the influence of gate electric fields.

Details for β – Sn Calculations

Bulk β – Sn: crystal structure

Bulk β -Sn has the tetragonal structure (A5) illustrated in Fig. 6 with a lattice constant of $a = 5.8179\text{\AA}$ and $c = 3.1749\text{\AA}$. This structure can be viewed as two body-center cubic structures displaced by a vector $\frac{1}{2}\mathbf{a} + \frac{1}{4}\mathbf{c}$ where \mathbf{a} and \mathbf{c} are the lattice vectors of the cubic unit cell. The lattice vectors of the primitive unit cell are $-\frac{1}{2}\mathbf{a} + \frac{1}{2}\mathbf{b} + \frac{1}{2}\mathbf{c}$, $\frac{1}{2}\mathbf{a} - \frac{1}{2}\mathbf{b} + \frac{1}{2}\mathbf{c}$ and $\frac{1}{2}\mathbf{a} + \frac{1}{2}\mathbf{b} - \frac{1}{2}\mathbf{c}$. There are two Sn atoms per cell with the positions as $(0, 0, 0)$ and $(\frac{1}{4}, \frac{3}{4}, \frac{1}{2})$ in crystal coordinates.

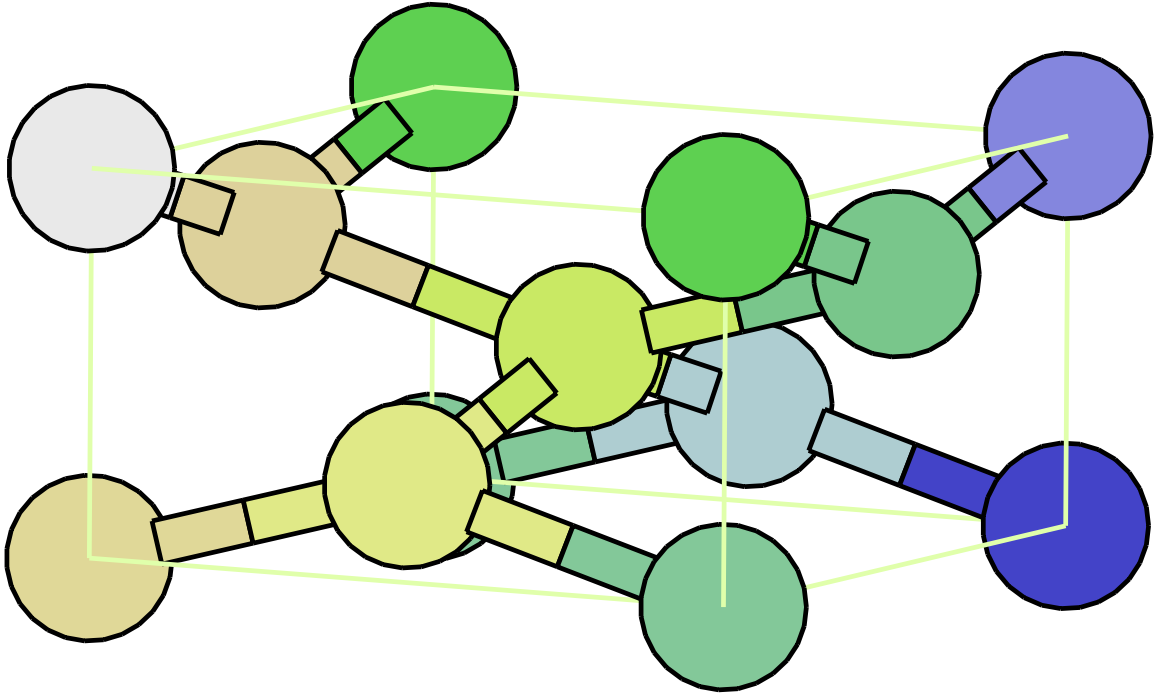


FIG. 6: Crystal structure of bulk β -Sn, which is a tetragonal structure (A5) with lattice constants $a = 5.8179\text{\AA}$ and $c = 3.1749\text{\AA}$.

The k-path used for the bulk β -Sn bandstructure plots in the main text is specified in Table II and in Fig. 7.

β – Sn 001 direction thin films: crystal structure

For thin film β -Sn, we choose the 001 growth direction. The lattice constant in the (001) direction is $a = 5.8197\text{\AA}$. To model the thin film we construct a supercell whose lattice vectors are $a\mathbf{x}$ and $a\mathbf{y}$ and $h\mathbf{z}$, where h is the height along z axis which is different from the lattice constant c of bulk β -Sn. In the calculations h is set to be the thickness of thin film plus a 20- \AA -thick vacuum layer. For the single Sn there are three Sn atoms per supercell with the positions as $(0, 0, 0)$, $(0.5, 0, \frac{c}{4h})$ and $(0.5, 0.5, \frac{c}{2h})$ in crystal coordinates, which form for the smallest unit cell a single layer where every atom is bonded. The structure of single layer is shown in Fig. 8.

TABLE II: Symmetry points in the first Brillouin zone of bulk β -Sn with a tetragonal structure (A5), with $\mathbf{k} = u\mathbf{a}^* + v\mathbf{b}^* + w\mathbf{c}^*$, where a^* , b^* , c^* are reciprocal lattice vectors shown as blue vectors in Fig. 7.

Symmetry points	k points:(u, v, w)
Γ	(0,0,0)
X	(0,0,0.5)
M	(-0.5,0.5,0.5)
P	(0.25,0.25,0.25)
N	(0,0.5,0)

The k -path of the bandstructure of thin film β -Sn in (001) direction in the main text is shown in table III and Fig. 9.

TABLE III: Symmetry points in the first Brillouin zone of thin film β -Sn in (001) direction, with $\mathbf{k} = u\mathbf{a}^* + v\mathbf{b}^* + w\mathbf{c}^*$, where a^* , b^* , c^* are reciprocal lattice vectors shown as blue vectors in Fig. 9.

Symmetry points	k points:(u, v, w)
Γ	(0,0,0)
M	(0.5,0,0)
X	(0.5,0.5,0)

Thin film β – Sn in 001 direction: electronic structure

More bandstructures of thin film β – Sn in 001 direction are shown in Fig.10a-10f, here we choose odd number of layers thin film up to 13 layers, the bands are mainly s and p orbitals, but s and p orbitals are highly hybridized for the layers more than 3, for the thicker thin film, more bands are hybridized, which makes the number of subbands much larger than the s and p bands.

Rashba constants

To extract the Rashba coupling constants we used the following equation:

$$\alpha_R \approx \frac{\Delta E}{\Delta k} \quad (1)$$

where Δk is chosen to be small enough. The Rashba coupling is of course band-dependent. Typical results are shown in Fig. 11, where the left side plots are for the bands closest to the Fermi level and the right sides is an average values over 12 subbands around the Fermi level: 6 above and 6 below. We see that the Rashba coupling becomes smaller when the number of layers increases. Up to 15 layers, however, its value is still up to $0.85 \text{ eV}\text{\AA}$, which is several times larger than in semiconductor quantum wires.

The influence of strain on Rashba coupling for 7,9 and 11 layers of Sn thin film is shown in Fig. 12: As it shows that tensile strain will weaken the Rashba effect while the compressive strain will strengthen the Rashba effect.

Details for Pb Calculations

Bulk Pb: cryatal structure

Bulk Pb has a face centered cubic structure as illustrated in Fig. 13 with a lattice constant of $a = 4.8408\text{\AA}$, The lattice vectors of the primitive unit cell are $\frac{1}{2}\mathbf{a} + \frac{1}{2}\mathbf{c}$, $\frac{1}{2}\mathbf{a} + \frac{1}{2}\mathbf{b}$ and $\frac{1}{2}\mathbf{b} + \frac{1}{2}\mathbf{c}$. In the primitive unit cell there is one Pb atom with the positions as (0, 0, 0) in crystal coordinates.

The k -path used to illustrate the bandstructure of bulk Pb in the main text is specified in table IV and in Fig. 14.

TABLE IV: Symmetry points in the first Brillouin zone of bulk Pb with a face centered cubic structure, with $\mathbf{k} = u\mathbf{a}^* + v\mathbf{b}^* + w\mathbf{c}^*$, where a^* , b^* , c^* are reciprocal lattice vectors shown as blue vectors in Fig. 14.

Symmetry points	k points:(u, v, w)
Γ	(0,0,0)
X	(0.5,0,0.5)
W	(0.5,0.25,0.75)
L	(0.5,0.5,0.5)
K	(0.375,0.375,0.75)

Thin film Pb in 111 direction: crystal structure

In the calculations for Pb thin films, we chose the bulk 111 direction as the film normal. The lattice constant is $a = 3.42\text{\AA}$ and the supercell constructed is similar with β -Sn film. The lattice vectors of the primitive unit cell used in the DFT calculation is $\frac{\sqrt{3}}{2}a\mathbf{x} + \frac{1}{2}a\mathbf{y}$ and $\frac{\sqrt{3}}{2}a\mathbf{x} + \frac{1}{2}a\mathbf{y}$, in which there are one Pb atom per cell located at (0,0,0) in crystal coordinates for the smallest unit cell of single layer. The structure of single layer is shown in Fig. 15.

The k-path used to illustrate the bandstructures of Pb thin films in the main text is shown in table V and Fig. 16.

TABLE V: Symmetry points in the first Brillouin zone of thin film Pb in (111) direction, with $\mathbf{k} = u\mathbf{a}^* + v\mathbf{b}^* + w\mathbf{c}^*$, where a^* , b^* , c^* are reciprocal lattice vectors shown as blue vectors in Fig. 16.

Symmetry points	k points:(u, v, w)
Γ	(0,0,0)
X	(0.5,0.5,0)
K	($\frac{1}{3}, \frac{2}{3}, 0$)

Thin film Pb in 111 direction: electronic structure

Here we selected several cases of Pb thin film to show the bandstructures, that is 3,5,7 and 9 layers thin film Pb in 111 direction, shown in Fig.17a-17d: A main difference from β -Sn thin film is that the hybridization of s orbital with p orbital is much smaller, and also an obvious quantum size effect has been shown, which has also been shown in the main text at Γ points. Another important difference is that in Pb thin film sp orbital has little hybridization with other orbitals such as d orbital, which give a smaller g-factor as show in the follow.

Pb(111) thin film on As_2O_3 substrates

To break the inversion symmetry of Pb thin film, we put it on a substrate of As_2O_3 . This choice is just a convenient theoretical model and other choices might be preferable experimentally. The As_2O_3 substrate has the Bi_2Te_3 structure. It is critical that the substrate be an insulator. Other possible substrates and their lattice constants are listed in table VI.

The crystal structure of a bilayer Pb (111) thin film as an example on As_2O_3 substrate is shown in Fig. 18, the lattice constant used come from Pb (111) thin film.

The k-path and symmetry points of the bandstructure of thin film Pb in (111) direction on a As_2O_3 substrate in the main text is shown in table VII and Fig. 19.

Pb(111) thin film on As_2O_3 substrate: Electronic structure

Electronic structure of 1-10 layers of Pb(111) thin film on As_2O_3 substrate are shown in Fig. 20: It can be seen that the bands of substrates are hybridized with subbands of Pb thin film, according to the main text, for the thin

TABLE VI: Lattice constants of Pb thin film in (111) direction and possible substrates.

Materials	Lattice constant (\AA)	Reference
Pb (111)	3.42	
Silicon (111)	3.84	
Bi ₂ Te ₃	4.3835	[72]
Bi ₂ Se ₃	4.138	[72]
Sb ₂ Te ₃	4.25	[72]
Sb ₂ Se ₃	4.076	[73]
MnAs(NiAs structure)	3.68	[74]
SrTiO ₃	3.905	[75]

TABLE VII: Symmetry points in the first Brillouin zone of thin film Pb in (111) direction on a As₂O₃ substrate, with $\mathbf{k} = u\mathbf{a}^* + v\mathbf{b}^* + w\mathbf{c}^*$, where a^* , b^* , c^* are reciprocal lattice vectors shown as blue vectors in Fig. 19.

Symmetry points	k points: (u, v, w)
Γ	(0,0,0)
X	(0.5,0,0)
K	$(\frac{1}{3}, \frac{1}{3}, 0)$

film with a strain around 2% the subband close to Fermi level has a small chemical potential, here we thus show the thin film with a strain around 2%, that the lattice constant is 4.9508 \AA .

To study the strain effect of substrates on the chemical potential, we calculated the band extremum from Fermi level at Γ point on As₂O₃ substrate, shown as in Fig. 21 for 5 and 10 layers of Pb thin film:

Rashba constants

The Rashba coupling constants vs the number of layers are shown as in Fig. 22, as it shows that the Rashba coupling becomes smaller when increasing the number of layers, and the average values of Rashba coupling around Fermi level is about 0.15 – 0.4eV \AA .

We also studied the strain effect on the Rashba effect, as an example the Rashba coupling for 5 and 10 layers of Pb thin film are shown in Fig. 23:

As it shows that tensile strain will strengthen the Rashba effect while the compressive strain will weaken the Rashba effect, which has an opposite effect compared with Sn film.

Pb(111) thin film on different substrates

Electronic Structure

To study the effect of substrates, we calculated the electronic structure of Pnictogen Chalcogenides substrates such as As₂O₃, Sb₂S₃, Sb₂Se₃, Bi₂Se₃, Bi₂Te₃, the results are shown in Fig.24 for 1 layer of Pb thin film.

For 2 layers of Pb thin film, the bandstructures are shown in Fig. 25: All of the calculations are done for the lattice constant of $a = 4.9508\text{\AA}$.

Rashba Coupling

To extract the Rashba splitting, the same methods are used as in Sn (001) thin film and Pb (111) thin film on As₂O₃ substrate. The Rashba coupling of 1 layer Pb (111) grown on different substrates are shown in Fig. 26a and 26b, while the Rashba coupling of 2 layer Pb (111) are shown in Fig. 26c and 26d. As the results show, the substrates with larger atom numbers will give a larger Rashba splitting.

Mean Field Theory

To analyse the class of topological phase for thin film metals, we construct a minimal mean field Hamiltonian. For the subbands around Fermi level, the minimal mean field Hamiltonian of the system can be written as:

$$H = \sum_{\mathbf{k}} \psi_{\mathbf{k}}^{\dagger} \mathcal{H}_{\mathbf{k}} \psi_{\mathbf{k}} \quad (2)$$

with the Nambu basis $\psi_{\mathbf{k}}^{\dagger} = [c_{\mathbf{k}\uparrow}^{\dagger}, c_{\mathbf{k}\downarrow}^{\dagger}, c_{-\mathbf{k}\uparrow}, c_{-\mathbf{k}\downarrow}]$ and

$$\begin{aligned} \mathcal{H}_{\mathbf{k}} = & \left(\frac{\hbar^2}{2m^*} \mathbf{k}^2 - \mu + g\mu_B B_x \sigma_x + g\mu_B B_z \sigma_z - \alpha_R k_x \sigma_y \right) \tau_z \\ & + \alpha_R k_y \sigma_x + g\mu_B B_y \sigma_y + \Delta (i\sigma_y) (i\tau_y) \end{aligned} \quad (3)$$

where m^* is the effective mass, μ is the chemical potential, α_R is the Rashba coupling constant, g is the g-factor, μ_B is the Bohr magneton, \mathbf{B} is the magnetic field, $\boldsymbol{\sigma}$ is the Pauli matrices acting on spin, $\boldsymbol{\tau}$ is the Pauli matrices acting on particle-hole space and Δ is the pairing potential of Cooper pairs.

For the time-reversal and particle-hole symmetry:

$$T = U_T \mathcal{K}, C = U_C \mathcal{K} \quad (4)$$

where \mathcal{K} is the conjugate operator and

$$U_T = i\sigma_y, U_C = \tau_x \quad (5)$$

it is obvious that:

$$T \mathcal{H}_{\mathbf{k}} T^{-1} \neq \mathcal{H}_{-\mathbf{k}}, C \mathcal{H}_{\mathbf{k}} C^{-1} = -\mathcal{H}_{-\mathbf{k}} \quad (6)$$

which shows that the system is a class D topological superconductivity in Altland-Zirnbauer system, for the reason of that $T^2 = -1$ and $C^2 = 1$. Since this is a 2D system, the topological invariant can be calculated with Chern number.

In real space, the mean field Hamiltonian is :

$$H = H_0 + H_R + H_{SC} + H_Z \quad (7)$$

with

$$H_0 = - \sum_{\langle ij \rangle, \sigma} t_{ij} c_{i\sigma}^{\dagger} c_{j\sigma} - \sum_{i, \sigma} \mu_i c_{i\sigma}^{\dagger} c_{j\sigma} \quad (8)$$

is the hopping term and chemical potential, where $t \approx \frac{\hbar^2}{2m^*a^2}$, where a is the effective lattice constant and

$$H_R = -\alpha \sum_j [c_{j-\hat{x},\downarrow}^{\dagger} c_{j,\uparrow} - c_{j+\hat{x},\downarrow}^{\dagger} c_{j,\uparrow} + i(c_{j-\hat{y},\downarrow}^{\dagger} c_{j,\uparrow} - c_{j+\hat{y},\downarrow}^{\dagger} c_{j,\uparrow}) + h.c.] \quad (9)$$

is the Rashba term with \hat{x} and \hat{y} the lattice vectors and $\alpha \approx \frac{\alpha_R}{a}$, and

$$H_{SC} = \sum_j (\Delta_j c_{j,\downarrow}^{\dagger} c_{j,\uparrow}^{\dagger} + h.c.) \quad (10)$$

is the s pairing superconductor and

$$H_Z = g\mu_B \sum_j c_j^{\dagger} \mathbf{B} \cdot \boldsymbol{\sigma} c_j \quad (11)$$

is the Zeeman term where $c_j^{\dagger} = [c_{j,\uparrow}^{\dagger}, c_{j,\downarrow}^{\dagger}]$

g-factor of thin film

The g-factors are obtained by evaluating the splitting between a Kramers pair at the Γ point under a magnetic field, which is[42]:

$$g(\mathbf{k}) = \frac{4m_e}{e\hbar} \frac{\partial \Delta E}{\partial \vec{B}} = \frac{4m_e}{e\hbar} \Delta\mu(\mathbf{k}) \quad (12)$$

where $\Delta\mu = \mu_1 - \mu_2$ and μ_i is the eigenvalues of the matrix $\hat{\mu}$, whose matrix elements are:

$$\mu_{n,\alpha\alpha'} = \mu_{n,\alpha\alpha'}^s + \mu_{n,\alpha\alpha'}^{or} \quad (13)$$

where the total contributions of the orbital part as

$$\mu_{n,\alpha\alpha'}^{or} = -\frac{e\hbar}{2i} \sum_{\alpha''=\alpha,\alpha'} \vec{a} \cdot \vec{v}_{n\alpha,n\alpha''} \times \Omega_{n\alpha'',n\alpha'}(\mathbf{k}) - \frac{e\hbar}{2i} \sum_{l \neq n,\alpha''} \vec{a} \cdot \frac{\vec{v}_{n\alpha,l\alpha''} \times \vec{v}_{l\alpha'',n\alpha'}}{E_n(\mathbf{k}) - E_l(\mathbf{k})} \quad (14)$$

where $\Omega_{n\alpha'',n\alpha'}(\mathbf{k}) = \langle u_{n\alpha''}(\mathbf{k}) | \frac{\partial}{\partial \mathbf{k}} | u_{n\alpha'}(\mathbf{k}) \rangle$, and the velocity elements are:

$$\vec{v}_{n\alpha,m\alpha'} = \frac{1}{\hbar} \langle u_{n\alpha}(\mathbf{k}) | \frac{\partial H}{\partial \mathbf{k}} | u_{m\alpha'}(\mathbf{k}) \rangle \quad (15)$$

the pure spin parts is

$$\mu_{n,\alpha\alpha'}^s = -\frac{e\hbar}{2m_e} \langle u_{n\alpha}(\mathbf{k}) | \vec{a} \cdot \vec{\sigma} | u_{n\alpha'}(\mathbf{k}) \rangle \quad (16)$$

where \vec{a} is the unit vector of direction of the magnetic field. According to Eq. 14, the density of subbands and velocity determined the value of g-factor, for this reason if the large hybridization between subbands will give a large g-factor. Also at Γ point, the velocity can be approximately determined by the Rashba coupling constant α_R (see Eq. 3), thus a large α_R usually gives a large g-factor.

As shown in Fig.27, as the film becomes thicker, the density of subbands becomes larger, while the Rashba coupling (shown as in Fig.11 and Fig. 22) becomes smaller, it is thus hard to estimate the trends of g-factor vs layers. From Fig.27 we can still get additional information about the subbands at Γ point and a large difference between Sn and Pb exists: that the hybridization of Sn thin film is larger, combined with the larger Rashba splitting of Sn thin film than Pb thin film, we can expect a larger g-factor in Sn thin film.

As Fig.28 and 29 show, we can see that the g-factors in Sn thin film are several times larger than the g-factors in Pb thin film, some oscillations happen in both Sn and Pb thin film, and the case of Sn thin film is even more complicated, although the quantum size effect has been studied in Pb thin film[58], there is no study on Sn thin film as the best of our knowledge, not only in theory but also in experiments. And all of the calculations show a greater prospective of Sn thin film than Pb thin film

to be a topological superconductor, that with a g-factor several times larger.

From Fig. 10 and 20 we can also see that at the Γ point, there are nearly degenerate subbands besides the Kramers pairs, this will give a extremely large g-factor values due to the diverge, to avoid this we do not consider these subbands when calculate the average value of g-factors. Although we did not calculate the g-factors under strain or with different substrates, we can give an approximate estimation according to the Rashba coupling, since under the strain or with different substrates the density of subbands keep almost the same, thus a larger Rashba coupling will give a larger g-factor.

* leichao.ph@gmail.com

- [1] C. Beenakker, Annu. Rev. Con. Mat. Phys. **4**, 113 (2013).
- [2] C. Beenakker and L. Kouwenhoven, Nat. Phys. **12**, 618 (2016).
- [3] A. Stern, Nature **464**, 187 (2010).
- [4] A. Jason, Rep. Prog. Phys. **75**, 076501 (2012).
- [5] L. Martin and F. Karsten, Semicond. Sci. Technol. **27**, 124003 (2012).
- [6] S. Masatoshi and A. Yoichi, Rep. Prog. Phys. **80**, 076501 (2017).
- [7] D. A. Ivanov, Phys. Rev. Lett. **86**, 268 (2001).
- [8] C. Nayak, S. H. Simon, A. Stern, M. Freedman, and S. Das Sarma, Rev. Mod. Phys. **80**, 1083 (2008).
- [9] A. Y. Kitaev, Phys. Usp. **44**, 131 (2001).
- [10] N. Read and D. Green, Phys. Rev. B **61**, 10267 (2000).
- [11] A. Das, Y. Ronen, Y. Most, Y. Oreg, M. Heiblum, and H. Shtrikman, Nat. Phys. **8**, 887 (2012).
- [12] M. T. Deng, C. L. Yu, G. Y. Huang, M. Larsson, P. Caroff, and H. Q. Xu, Nano Lett. **12**, 6414 (2012).
- [13] V. Mourik, K. Zuo, S. M. Frolov, S. R. Plissard, E. P. A. M. Bakkers, and L. P. Kouwenhoven, Science **336**, 1003 (2012).

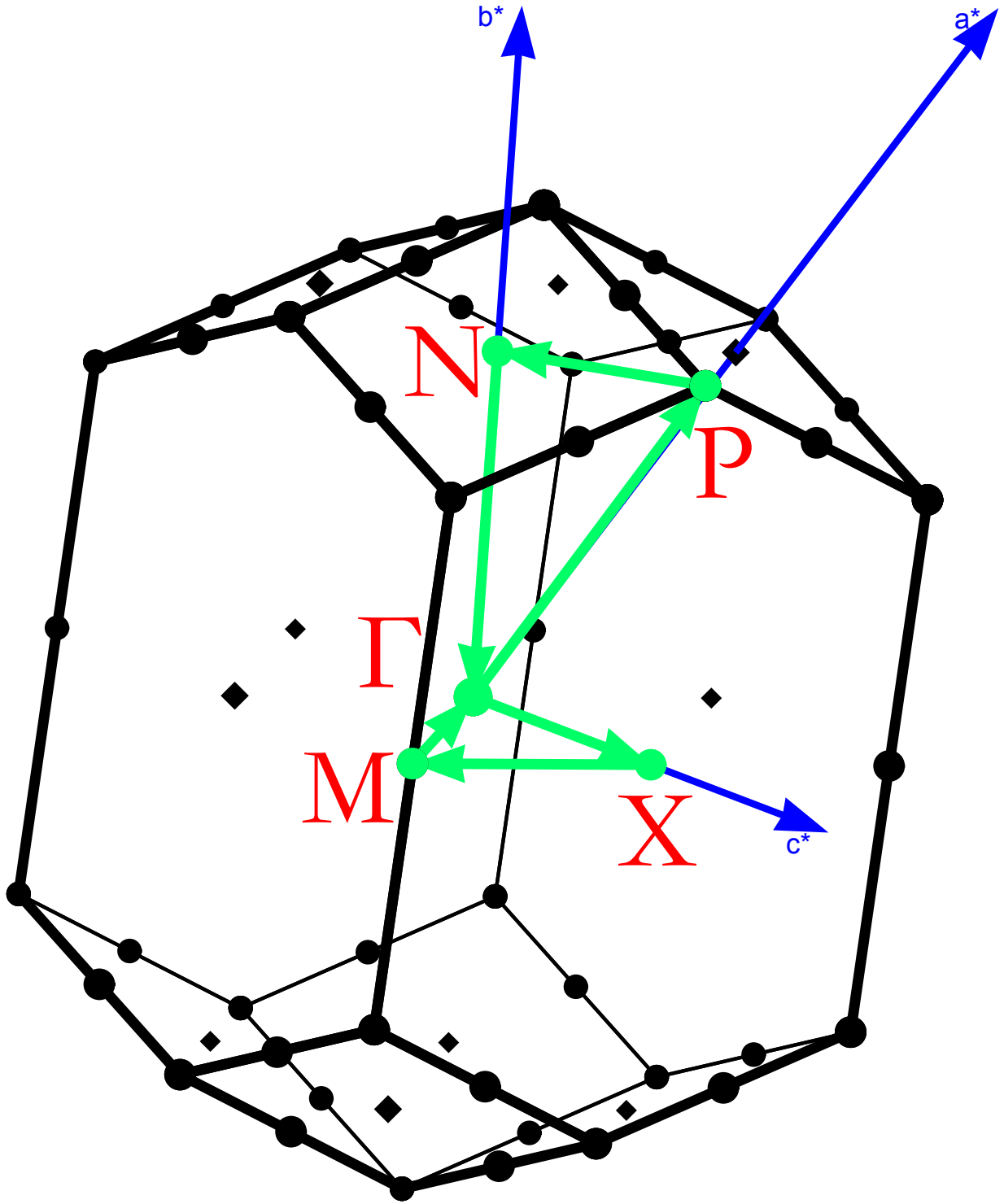


FIG. 7: The first Brillouin zone and the k-path selected to illustrate the bandstructure of bulk β -Sn. The points labelled in red are the plotted high symmetry points and the green lines are the connecting paths.

- [14] L. P. Rokhinson, X. Liu, and J. K. Furdyna, *Nat. Phys.* **8**, 795 (2012).
- [15] R. M. Lutchyn, J. D. Sau, and S. Das Sarma, *Phys. Rev. Lett.* **105**, 077001 (2010).
- [16] J. D. Sau, R. M. Lutchyn, S. Tewari, and S. Das Sarma, *Phys. Rev. Lett.* **104**, 040502 (2010).
- [17] S. M. Albrecht, A. P. Higginbotham, M. Madsen, F. Kuemmeth, T. S. Jespersen, J. Nygrd, P. Krogstrup, and C. M. Marcus, *Nature* **531**, 206 (2016).
- [18] M. T. Deng, S. Vaitieknas, E. B. Hansen, J. Danon, M. Leijnse, K. Flensberg, J. Nygrd, P. Krogstrup, and C. M. Marcus, *Science* **354**, 1557 (2016).

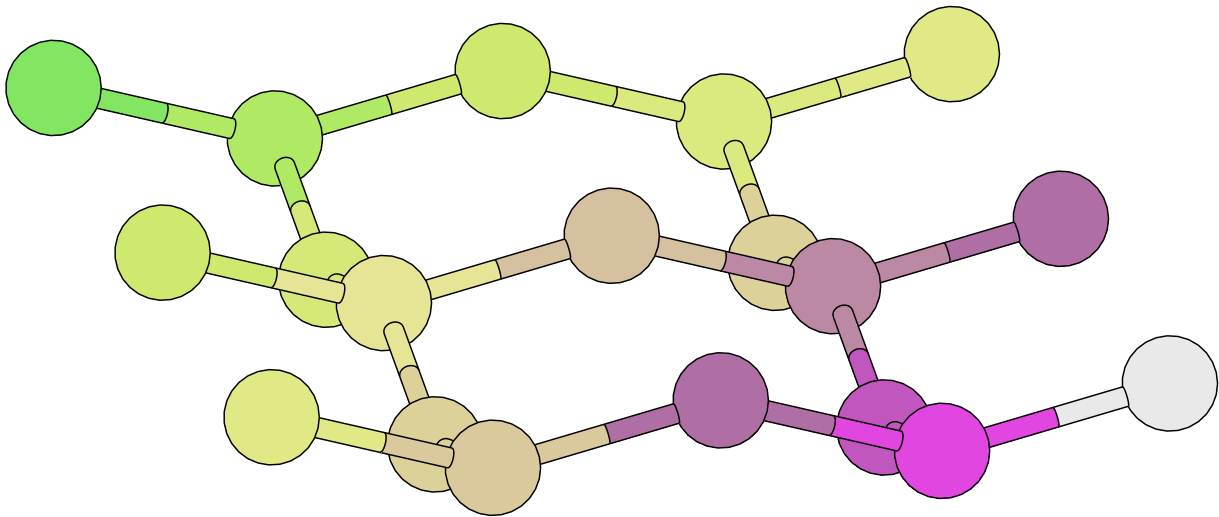


FIG. 8: Crystal structure of thin film β -Sn in (001) direction, the lattice constant is $a = 5.8197\text{\AA}$.

- [19] S. Nadj-Perge, I. K. Drozdov, J. Li, H. Chen, S. Jeon, J. Seo, A. H. MacDonald, B. A. Bernevig, and A. Yazdani, *Science* **346**, 602 (2014).
- [20] B. E. Feldman, M. T. Randeria, J. Li, S. Jeon, Y. Xie, Z. Wang, I. K. Drozdov, B. Andrei Bernevig, and A. Yazdani, *Nat. Phys.* **13**, 286 (2016).
- [21] R. Pawlak, M. Kisiel, J. Klinovaja, T. Meier, S. Kawai, T. Glatzel, D. Loss, and E. Meyer, *npj Quantum Information* **2**, 16035 (2016).
- [22] Q. L. He, L. Pan, A. L. Stern, E. C. Burks, X. Che, G. Yin, J. Wang, B. Lian, Q. Zhou, E. S. Choi, K. Murata, X. Kou, Z. Chen, T. Nie, Q. Shao, Y. Fan, S.-C. Zhang, K. Liu, J. Xia, and K. L. Wang, *Science* **357**, 294 (2017).
- [23] Y. Zeng, C. Lei, G. Chaudhary, and A. H. MacDonald, *Phys. Rev. B* **97**, 081102 (2018).
- [24] N. Mohanta and A. Taraphder, *EPL (Europhysics Letters)* **108**, 60001 (2014).
- [25] M. S. Scheurer and J. Schmalian, *Nature communications* **6**, 6005 (2015).
- [26] F. Loder, A. P. Kampf, and T. Kopp, *Scientific reports* **5**, 15302 (2015).
- [27] T. Tzen Ong and P. Coleman, *Phys. Rev. B* **90**, 174506 (2014).
- [28] M. S. Scheurer, D. F. Agterberg, and J. Schmalian, *npj Quantum Materials* **2**, 9 (2017).
- [29] M. S. Scheurer, *Phys. Rev. B* **93**, 174509 (2016).
- [30] K. V. Samokhin, *Phys. Rev. B* **92**, 174517 (2015).
- [31] Y. Wang, G. Y. Cho, T. L. Hughes, and E. Fradkin, *Phys. Rev. B* **93**, 134512 (2016).
- [32] F. Loder, A. P. Kampf, T. Kopp, and D. Braak, *Phys. Rev. B* **96**, 024508 (2017).
- [33] N. Wernerdal and M. Eschrig, *Phys. Rev. B* **95**, 024513 (2017).
- [34] G. Cheng, M. Tomczyk, S. Lu, J. P. Veazey, M. Huang, P. Irvin, S. Ryu, H. Lee, C.-B. Eom, C. S. Hellberg, *et al.*, *Nature* **521**, 196 (2015).
- [35] C. Brun, T. Cren, and D. Roditchev, *Supercond. Sci. Technol* **30**, 013003 (2016).
- [36] H. Nam, H. Chen, T. Liu, J. Kim, C. Zhang, J. Yong, T. R. Lemberger, P. A. Kratz, J. R. Kirtley, K. Moler, P. W. Adams, A. H. MacDonald, and C.-K. Shih, *Proc. Natl. Acad. Sci. USA* **113**, 10513 (2016).
- [37] T. Zhang, P. Cheng, W.-J. Li, Y.-J. Sun, G. Wang, X.-G. Zhu, K. He, L. Wang, X. Ma, X. Chen, Y. Wang, Y. Liu, H.-Q. Lin, J.-F. Jia, and Q.-K. Xue, *Nature Physics* **6**, 104 (2010).
- [38] G. C. Menard, S. Guissart, C. Brun, R. T. Leriche, M. Trif, F. Debontridder, D. Demaille, D. Roditchev, P. Simon, and T. Cren, *Nat. Comm.* **8**, 2040 (2017).
- [39] A. C. Potter and P. A. Lee, *Phys. Rev. B* **85**, 094516 (2012).
- [40] L. Yan-Feng, W. Wen-Lin, Z. Yi-Min, D. Hao, L. Wei, W. Lili, H. Ke, S. Can-Li, M. Xu-Cun, and X. Qi-Kun, *Sci. Bull.* **62**, 852 (2017).
- [41] See Supplemental Material at [URL] for more information.
- [42] C. Lei, H. Chen, and A. H. MacDonald, to be published.
- [43] C.-K. Chiu, J. C. Y. Teo, A. P. Schnyder, and S. Ryu, *Rev. Mod. Phys.* **88**, 035005 (2016).
- [44] R. L. Hota, G. S. Tripathi, and J. N. Mohanty, *Phys. Rev. B* **47**, 9319 (1993).
- [45] R. Patnaik and G. Tripathi, *Solid State Commun.* **112**, 669 (1999).
- [46] M. Debessai, T. Matsuoka, J. J. Hamlin, W. Bi, Y. Meng, K. Shimizu, and J. S. Schilling, *J. Phys.: Confer. Series* **215**, 012034 (2010).
- [47] J. Eisenstein, *Rev. Mod. Phys.* **26**, 277 (1954).
- [48] G. P. Mikitik and Y. V. Sharlai, *Phys. Rev. B* **67**, 115114 (2003).
- [49] D. Xiao, J. Shi, and Q. Niu, *Phys. Rev. Lett.* **95**, 137204 (2005).
- [50] T. Thonhauser, D. Ceresoli, D. Vanderbilt, and R. Resta, *Phys. Rev. Lett.* **95**, 137205 (2005).
- [51] M. Miasek, *Phys. Rev.* **130**, 11 (1963).
- [52] J. E. Craven, *Phys. Rev.* **182**, 693 (1969).
- [53] A. D. Zdetsis, E. N. Economou, and D. A. Papaconstantopoulos, *J. Phys. F* **10**, 1149 (1980).
- [54] M. E. Woods and B. J. Hopkins, *J. Phys. C* **18**, 217 (1985).
- [55] B. Slomski, G. Landolt, S. Muff, F. Meier, J. Osterwalder, and J. H. Dil, *New J. Phys.* **15**, 125031 (2013).

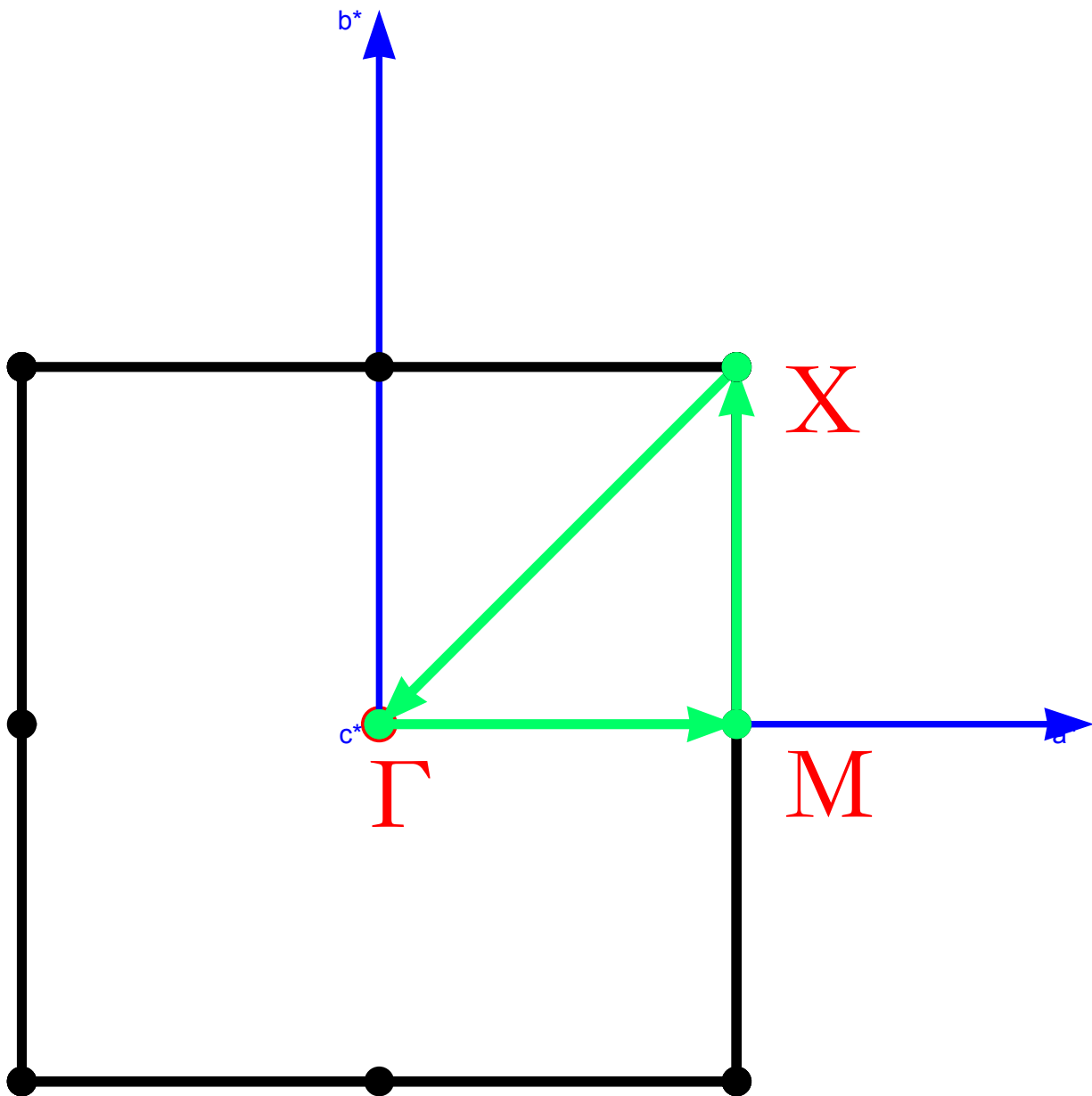
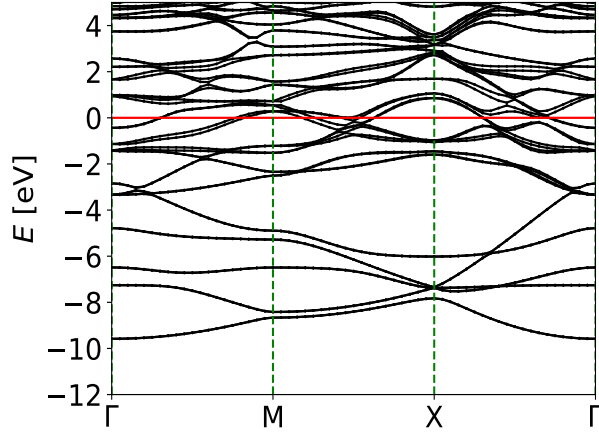
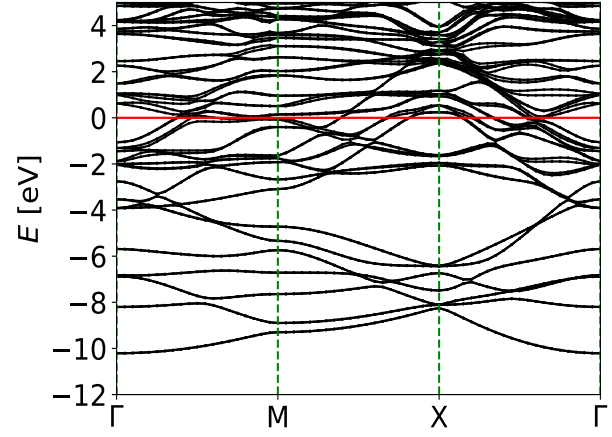


FIG. 9: The first Brillouin zone and the k-path used to calculate the bandstructure of the thin film β -Sn in (001) direction.

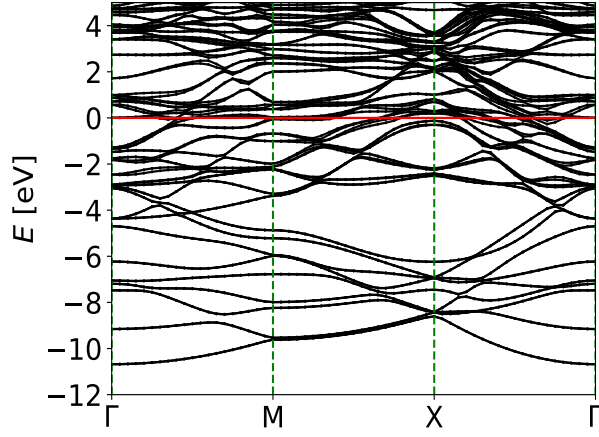
- [56] J. H. Dil, F. Meier, J. Lobo-Checa, L. Patthey, G. Bihlmayer, and J. Osterwalder, *Phys. Rev. Lett.* **101**, 266802 (2008).
- [57] L. Florian, P. K. Arno, and K. Thilo, *J. Phys. Condens. Matter* **25**, 362201 (2013).
- [58] C. M. Wei and M. Y. Chou, *Phys. Rev. B* **66**, 233408 (2002).
- [59] M. Oshiki and E. Fukada, *J. Mater. Sci.* **10**, 1 (1975).
- [60] D. E. Grupp and A. M. Goldman, *Science* **276**, 392 (1997).
- [61] Z. Zhang, Q. Niu, and C.-K. Shih, *Phys. Rev. Lett.* **80**, 5381 (1998).
- [62] M. Murakami and R. W. Vook, *Crit. Rev. Solid State Mater. Sci.* **11**, 317 (1983).
- [63] P. Giannozzi, S. Baroni, N. Bonini, M. Calandra, R. Car, C. Cavazzoni, D. Ceresoli, G. L. Chiarotti, M. Cococcioni, I. Dabo, A. Dal Corso, S. de Gironcoli, S. Fabris, G. Fratesi, R. Gebauer, U. Gerstmann, C. Gougoussis, A. Kokalj, M. Lazzeri, L. Martin-Samos, N. Marzari, F. Mauri, R. Mazzarello, S. Paolini, A. Pasquarello, L. Paulatto, C. Sbraccia, S. Scandolo, G. Sclauzero, A. P. Seitsonen, A. Smogunov, P. Umari, and R. M. Wentzcovitch, *J. Phys. Condens. Matter* **21**, 395502 (19pp) (2009).
- [64] P. Giannozzi, O. Andreussi, T. Brumme, O. Bunau, M. B. Nardelli, M. Calandra, R. Car, C. Cavazzoni, D. Ceresoli, M. Cococcioni, N. Colonna, I. Carnimeo, A. D. Corso, S. de Gironcoli, P. Delugas, R. A. D. Jr, A. Ferretti, A. Floris, G. Fratesi, G. Fugallo, R. Gebauer,



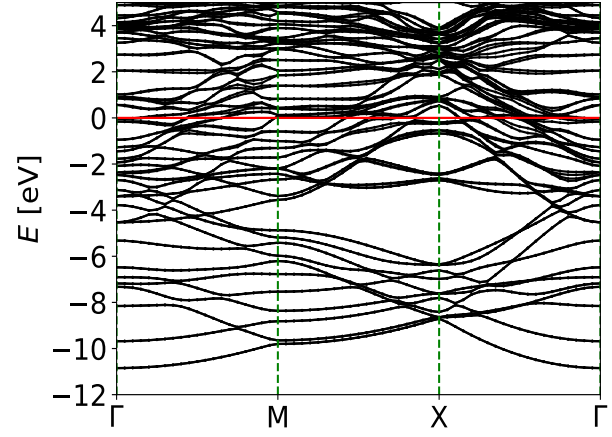
(a) 3 Layer of Sn (001)



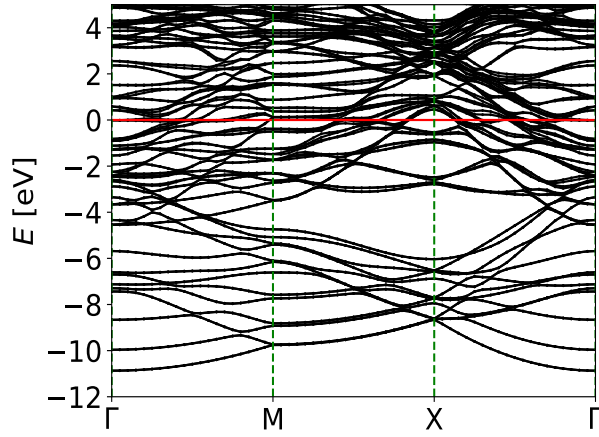
(b) 5 Layer of Sn (001)



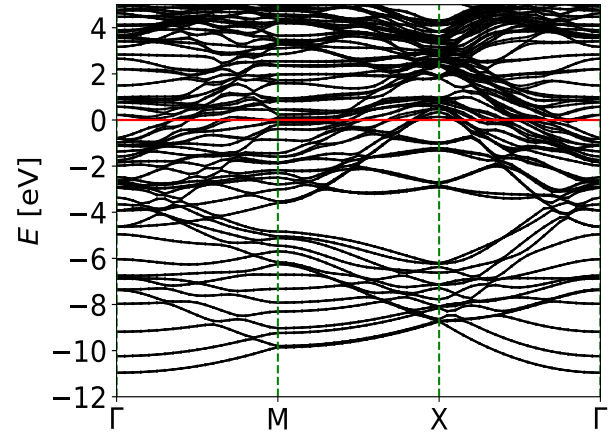
(c) 7 Layer of Sn (001)



(d) 9 Layer of Sn (001)

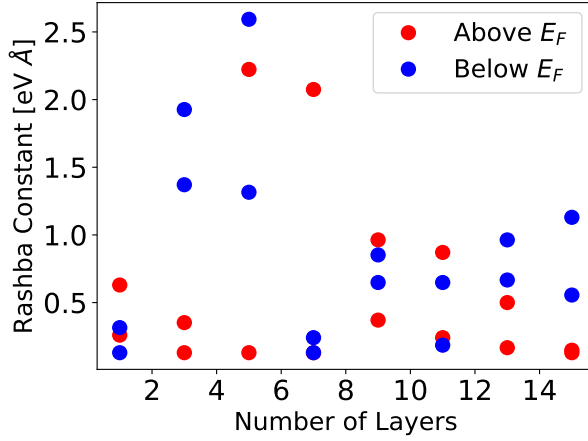


(e) 11 Layer of Sn (001)

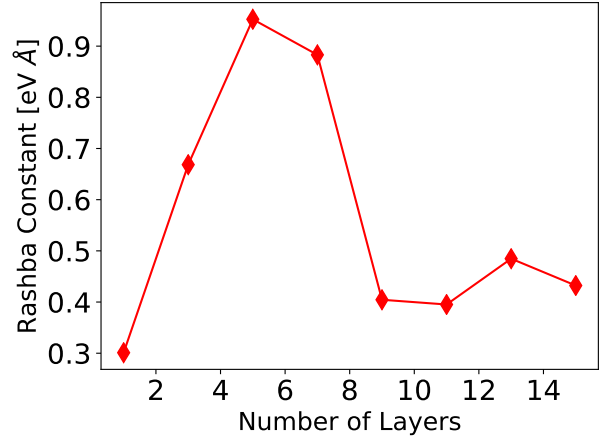


(f) 13 Layer of Sn (001)

FIG. 10: Band structure of thin film β Sn grown along the (001) direction, from a 3 layers (5 atomic layer) to 13 layers



(a) Rashba coupling of Sn (001) vs layers



(b) Average Rashba coupling of Sn (001) vs layers

FIG. 11: Rashba coupling (and the average of 10 bands around Fermi level) of Sn (001) around Fermi level vs layers

U. Gerstmann, F. Giustino, T. Gorni, J. Jia, M. Kawamura, H.-Y. Ko, A. Kokalj, E. Kkbenli, M. Lazzeri, M. Marsili, N. Marzari, F. Mauri, N. L. Nguyen, H.-V. Nguyen, A. O. de-la Roza, L. Paulatto, S. Ponc, D. Rocca, R. Sabatini, B. Santra, M. Schlipf, A. P. Seitsonen, A. Smogunov, I. Timrov, T. Thonhauser, P. Umari, N. Vast, X. Wu, and S. Baroni, *J. Phys. Condens. Matter* **29**, 465901 (2017).

[65] A. Dal Corso, *Comput. Mater. Sci* **95**, 337 (2014).

[66] G. Kresse and J. Hafner, *Phys. Rev. B* **47**, 558 (1993).

[67] G. Kresse and J. Hafner, *Phys. Rev. B* **49**, 14251 (1994).

[68] G. Kresse and J. Furthmüller, *Comput. Mater. Sci* **6**, 15 (1996).

[69] G. Kresse and J. Furthmüller, *Phys. Rev. B* **54**, 11169 (1996).

[70] J. P. Perdew, K. Burke, and M. Ernzerhof, *Phys. Rev. Lett.* **77**, 3865 (1996).

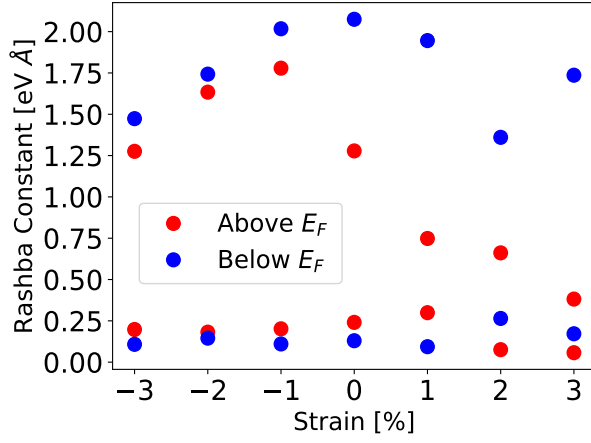
[71] J. P. Perdew, K. Burke, and M. Ernzerhof, *Phys. Rev. Lett.* **78**, 1396 (1997).

[72] “Bismuth telluride (bi2te3) crystal structure, chemical bond, lattice parameters (including data for related compounds): Datasheet from landolt-brnstein - group iii condensed matter volume 41c: ”non-tetrahedrally bonded elements and binary compounds i” in springermaterials,”.

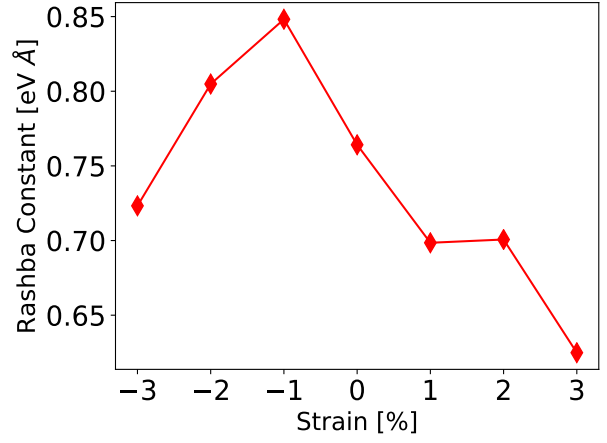
[73] H. Zhang, C.-X. Liu, X.-L. Qi, X. Dai, Z. Fang, and S.-C. Zhang, *Nat. Phys.* **5**, 438 (2009).

[74] K. Motizuki, H. Ido, T. Itoh, and M. Morifuji, (2009).

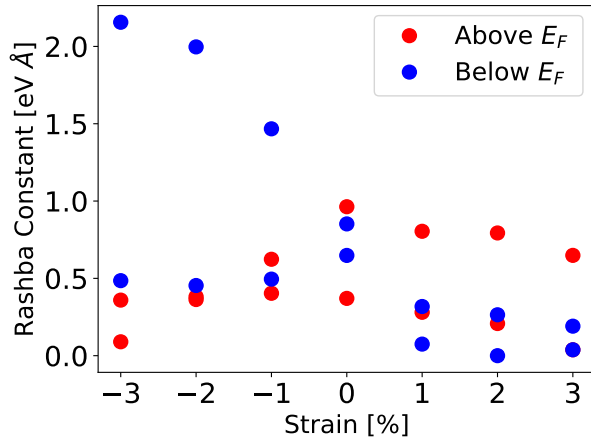
[75] “SrTiO3 crystal structure, lattice parameters: Datasheet from landolt-brnstein - group iii condensed matter volume 41e: ”ternary compounds, organic semiconductors” in springermaterials,”.



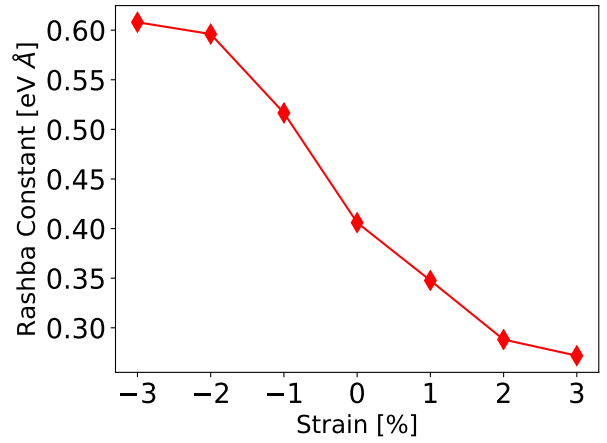
(a) Rashba coupling of Sn (001) vs strain for 7 layers case



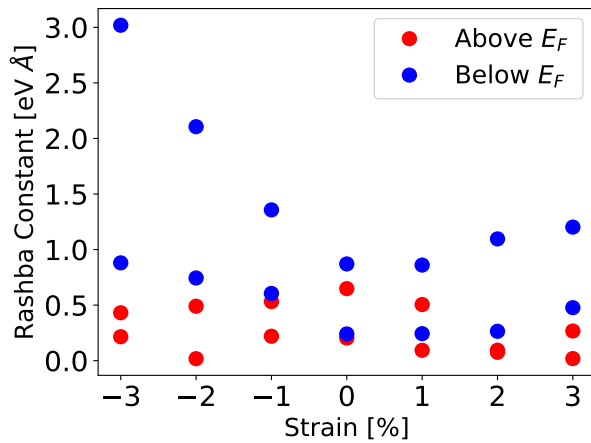
(b) Average Rashba coupling of Sn (001) vs strain for 7 layers case



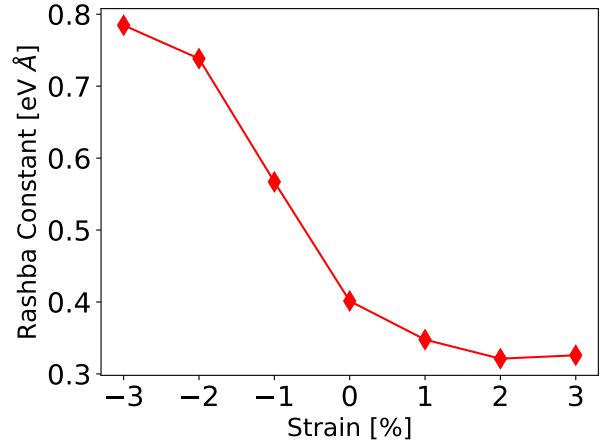
(c) Rashba coupling of Sn (001) vs strain for 9 layers case



(d) Average Rashba coupling of Sn (001) vs strain for 9 layers case



(e) Rashba coupling of Sn (001) vs strain for 11 layers case



(f) Average Rashba coupling of Sn (001) vs strain for 11 layers case

FIG. 12: Rashba coupling (and the average of 12 bands around Fermi level) of Sn (001) around Fermi level vs strain for 7, 9 and 11 layers case.

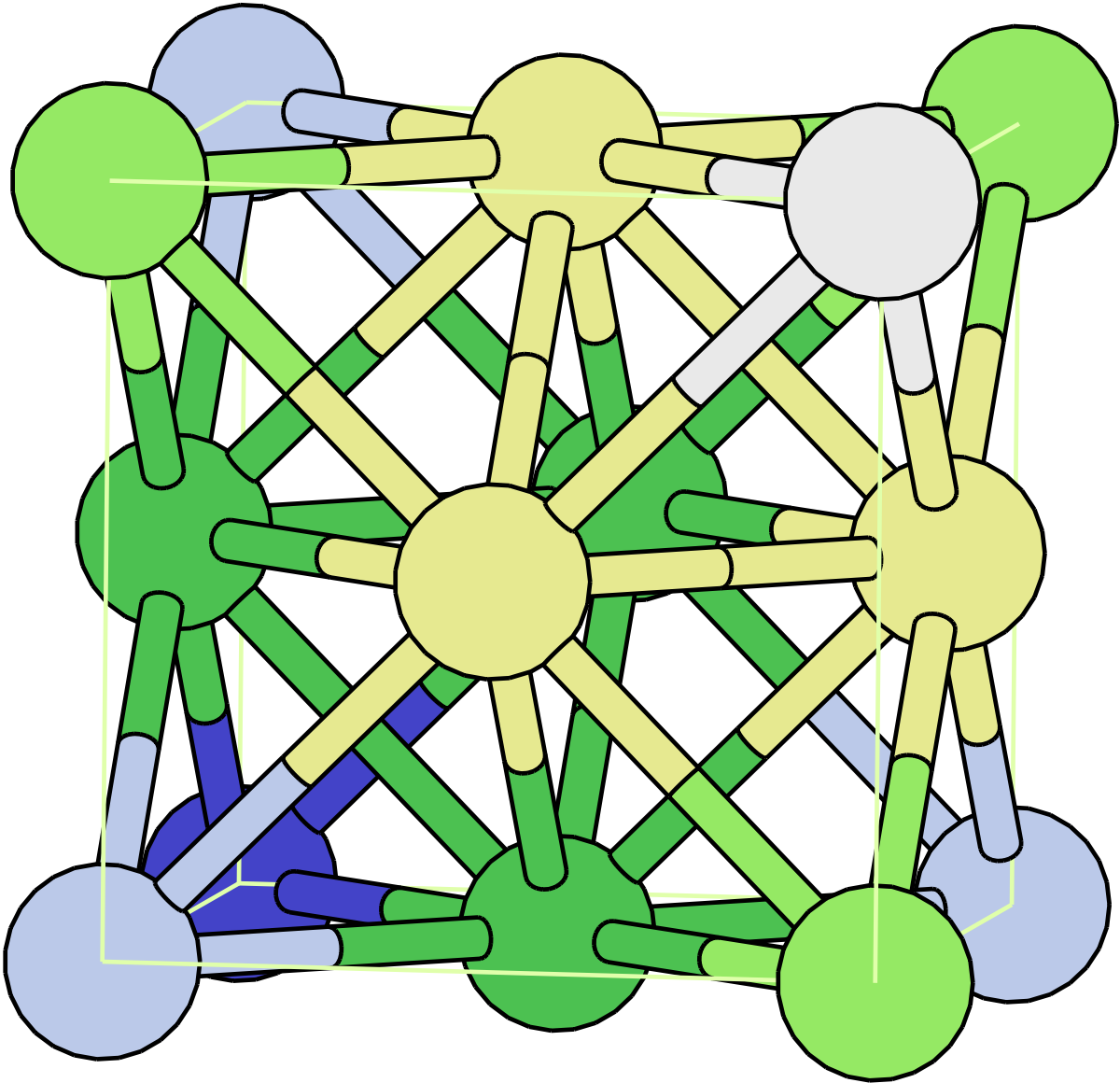


FIG. 13: Crystal structure of face centered cubic bulk Pb with a lattice constant of $a = 4.8408\text{\AA}$

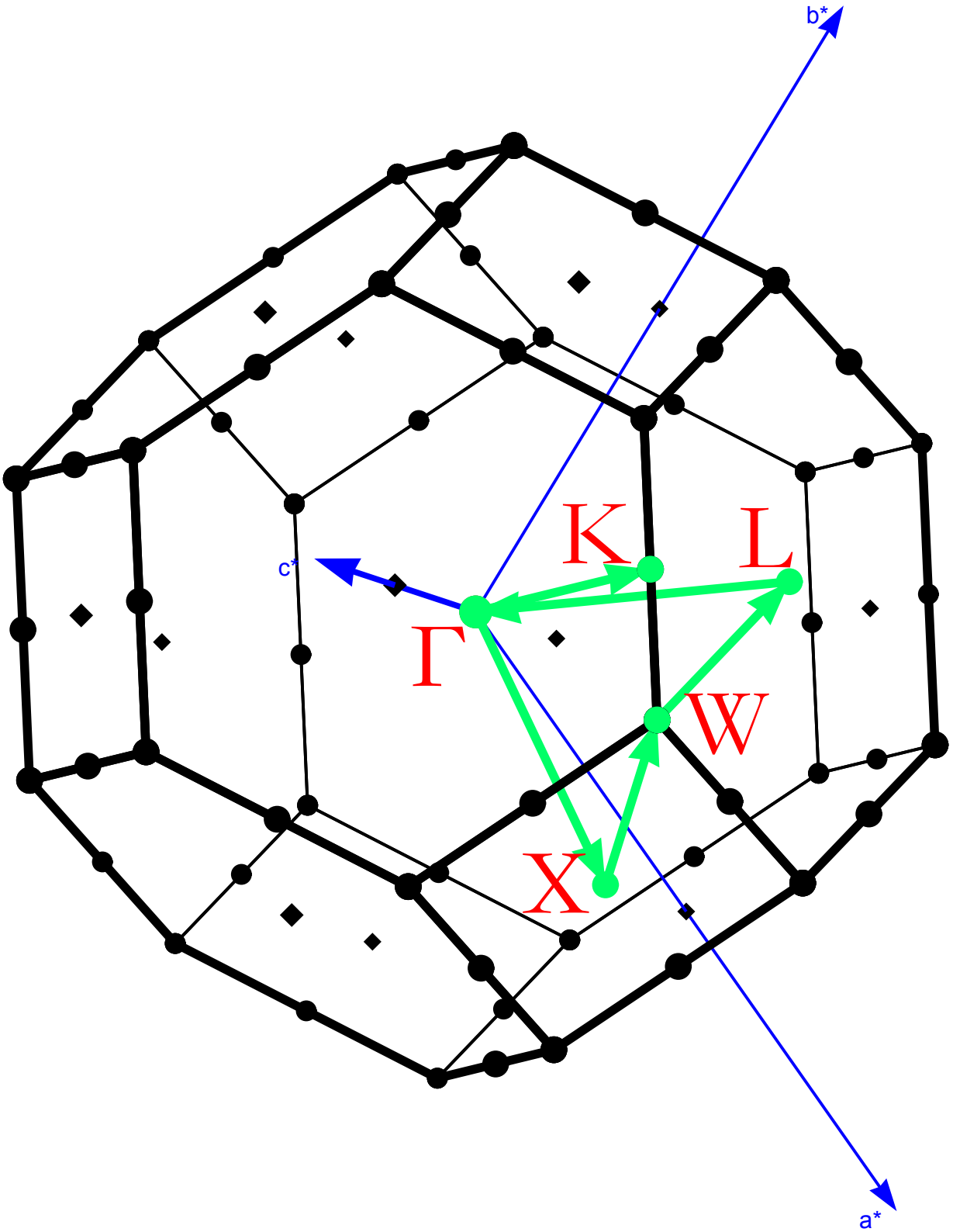


FIG. 14: The first Brillouin zone of bulk Pb with face centered cubic structure and the k-path used in the main text to illustrate the bandstructure. The green lines are the symmetry paths used to connect high symmetry points labelled in red.

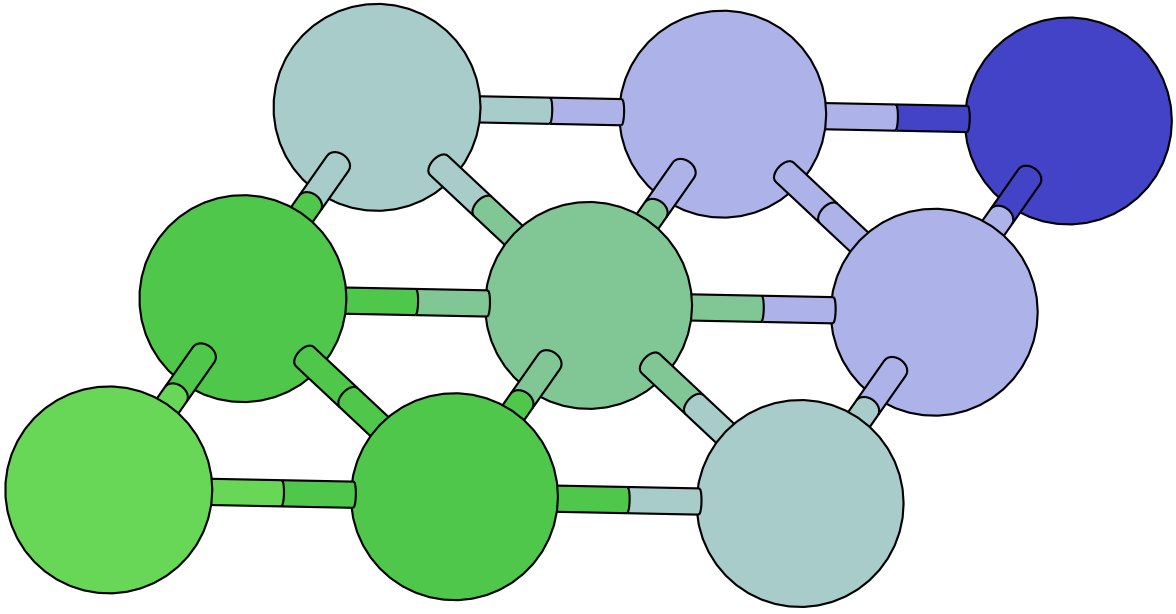


FIG. 15: Crystal structure of thin film Pb, whose in-plane lattice constant is the same as that of bulk Pb, $a = 3.42\text{\AA}$.

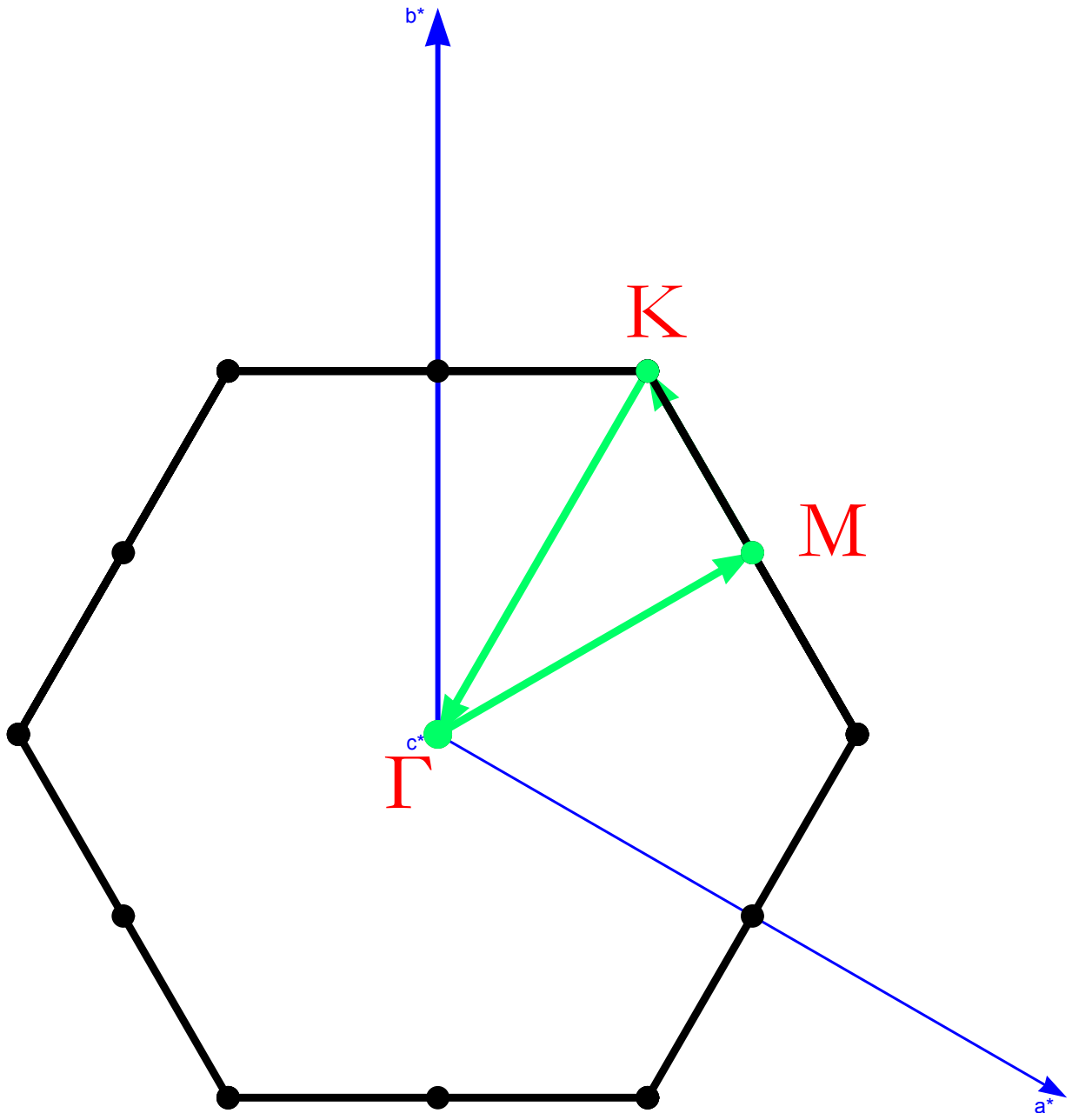
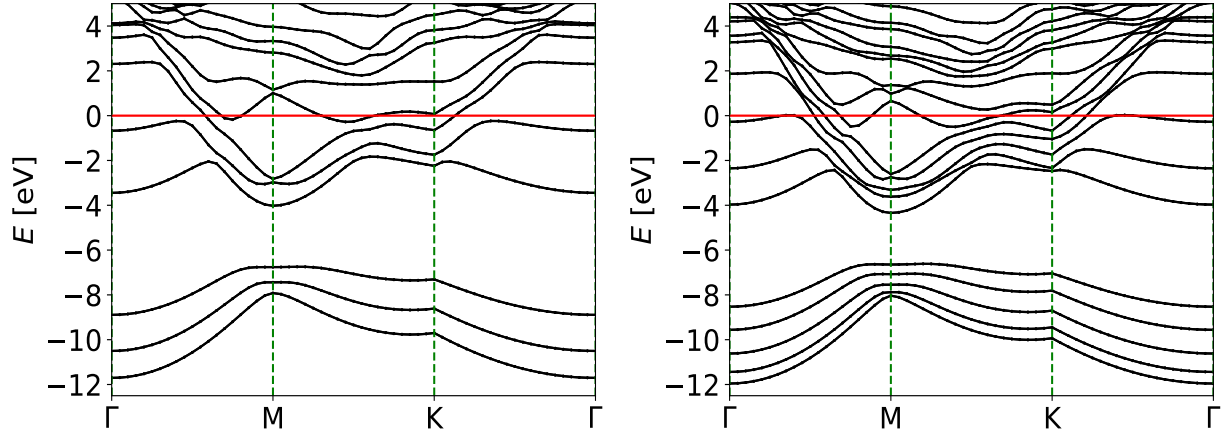
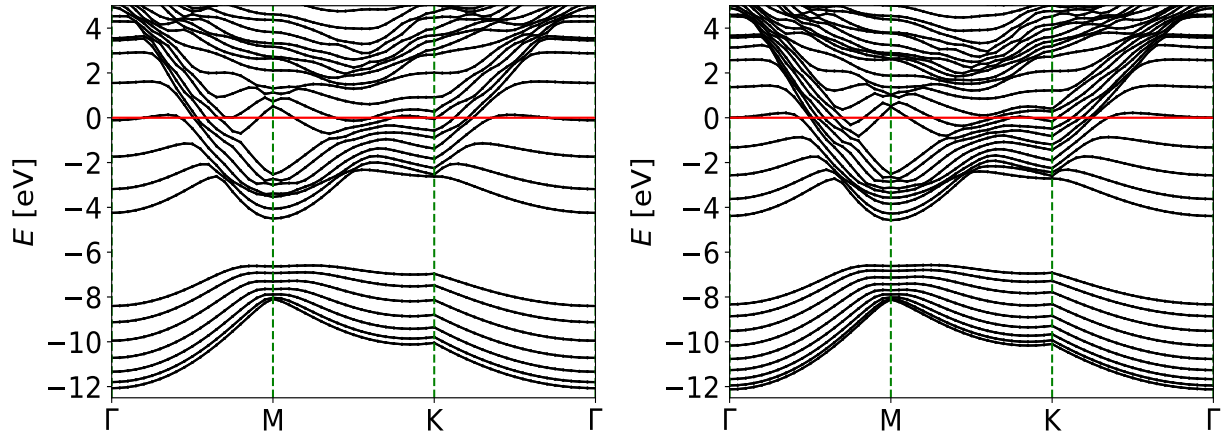


FIG. 16: The first Brillouin zone of (111) growth direction Pb thin films and the k-path used to calculate the bandstructure in the main text. The k-path is labeled with green lines and the symmetry points are indicated by red letters.



(a) 3 Layers of Pb (111)

(b) 5 Layers of Pb (111)



(c) 7 Layers of Pb (111)

(d) 9 Layers of Pb (111)

FIG. 17: Selected bandstructure of a thin film Pb grown along the (111) direction: 3,5,7,9 layers

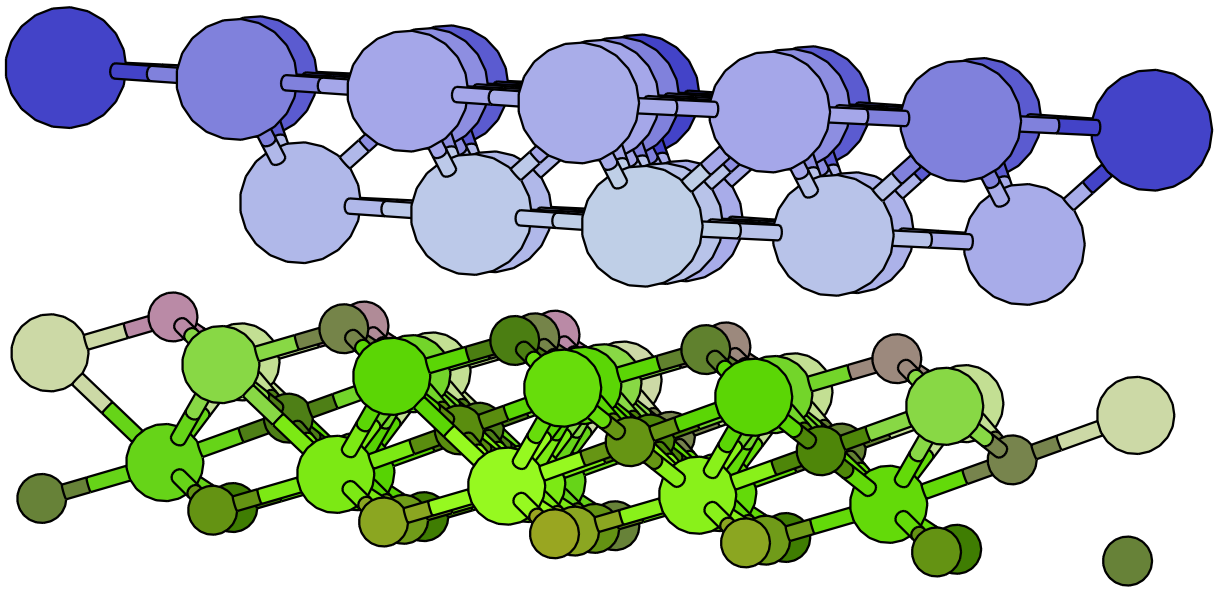


FIG. 18: Crystal structure of thin film Pb in (111) direction on As_2O_3 substrate with Bi_2Te_3 structure, where blue slab on the top is the Pb thin film and the green slab on the bottom is the As_2O_3 substrate. The lattice constant used come from Pb.

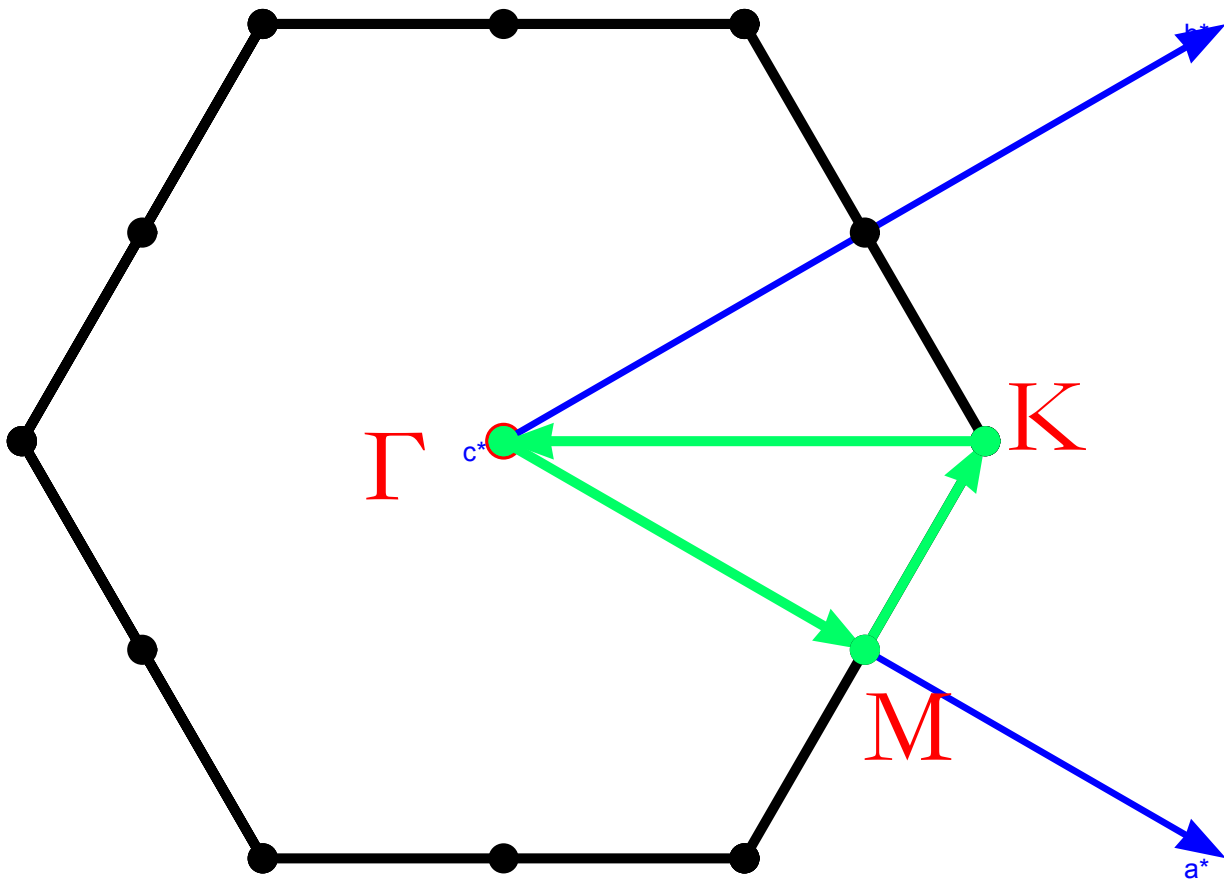


FIG. 19: The first Brillouin zone of thin film Pb in (111) direction on a As_2O_3 substrate. The k-path is labeled with green lines and the symmetry points are indicated by red letters.

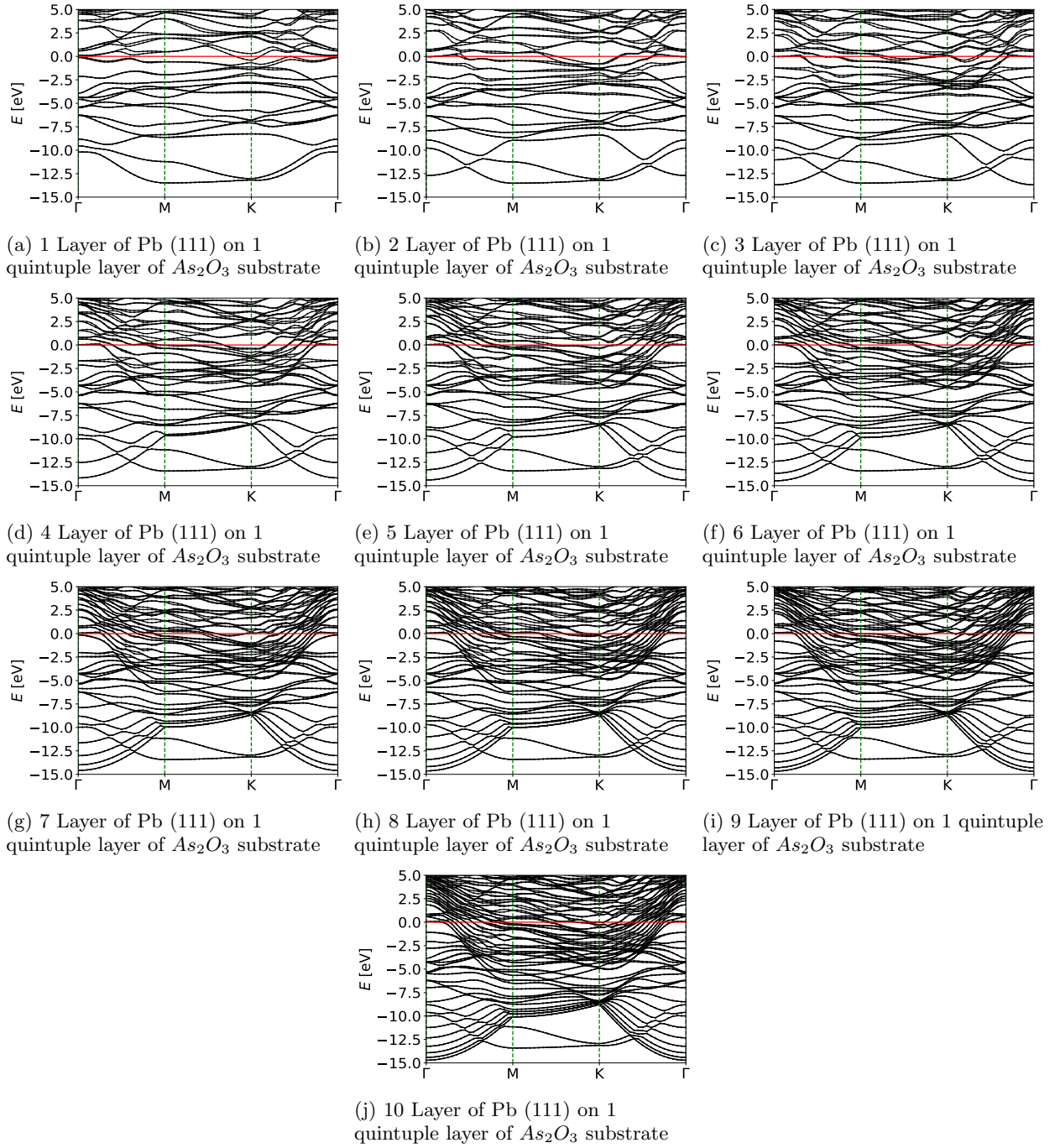


FIG. 20: Band structure of Pb thin film in (111) direction grown on 1 quintuple layer of As_2O_3 substrate: 1-10 layers of Pb thin film

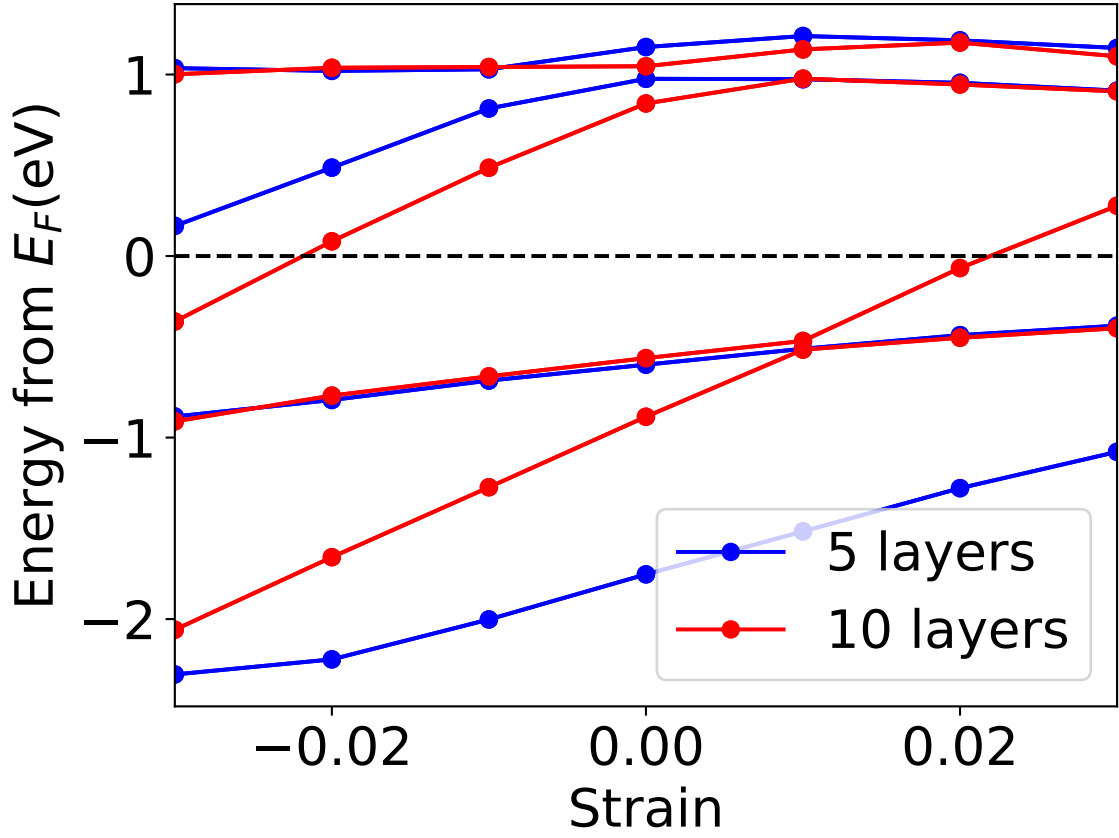
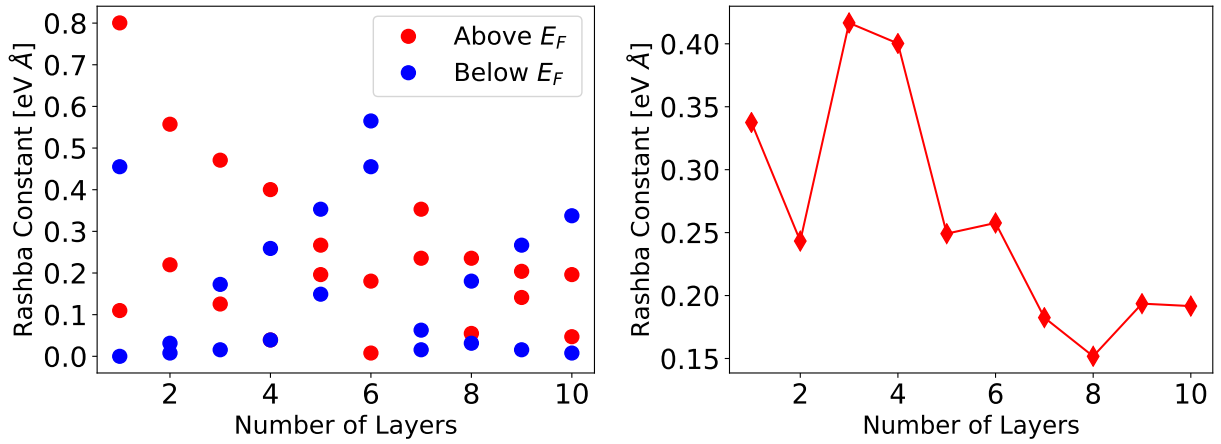


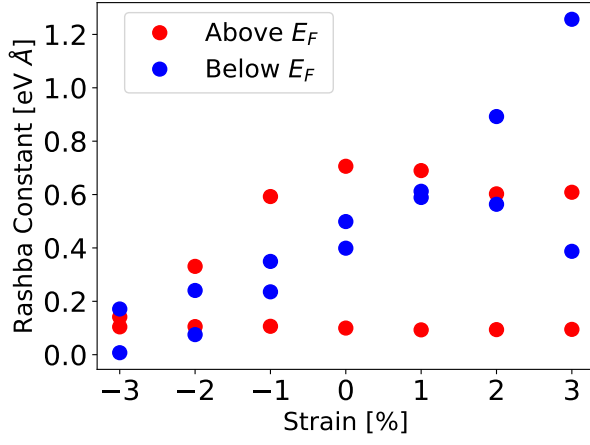
FIG. 21: Strain dependence of energy separations between quasi-2D band extrema at Γ point and Fermi energies for Pb (111) thin film on As_2O_3 substrate



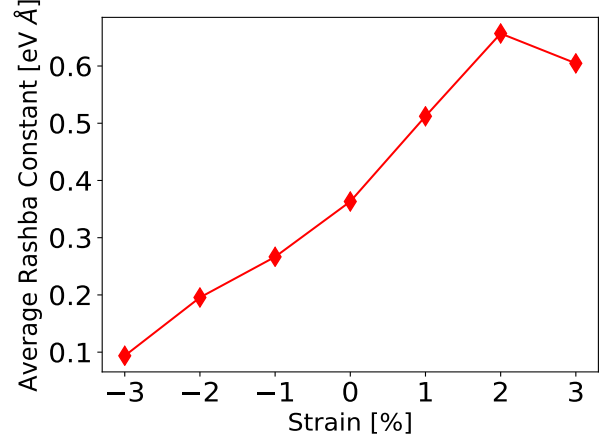
(a) Rashba coupling of Pb (111) vs layers

(b) Average Rashba coupling of Pb (111) vs layers

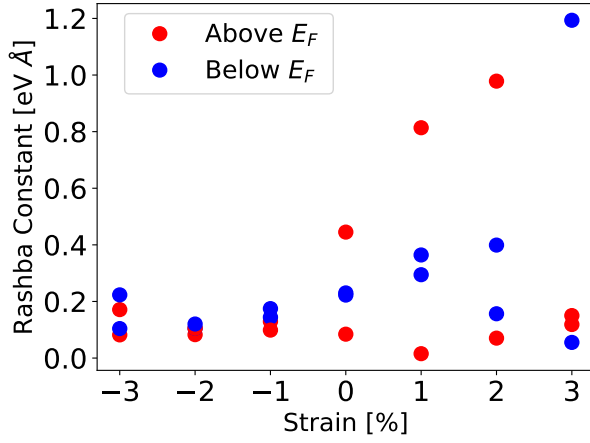
FIG. 22: Rashba coupling (and the average of 10 bands around Fermi level) of Pb (111) around Fermi level vs layers



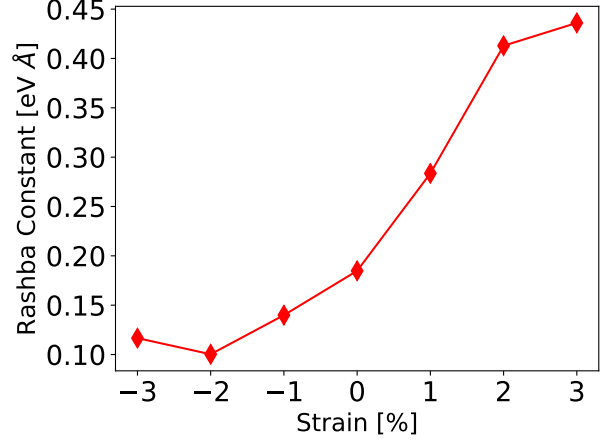
(a) Rashba coupling of Pb (111) vs strain for 5 layers case



(b) Average Rashba coupling of Pb (111) vs strain for 5 layers case

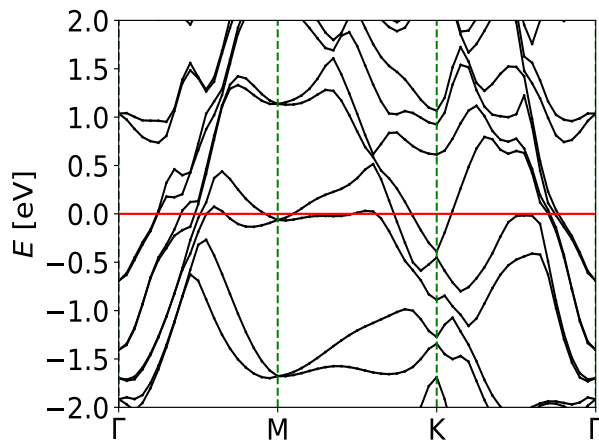


(c) Rashba coupling of Pb (111) vs strain for 10 layers case

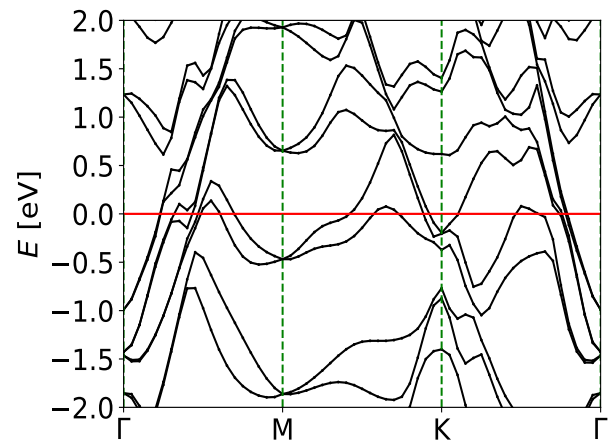


(d) Average Rashba coupling of Pb (111) vs strain for 10 layers case

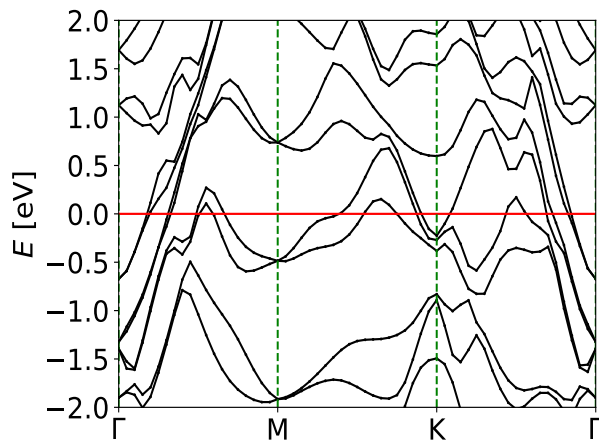
FIG. 23: Rashba coupling (and the average of 12 bands around Fermi level) of Pb (111) around Fermi level vs strain for 5 and 10 layers case on As_2O_3 substrates.



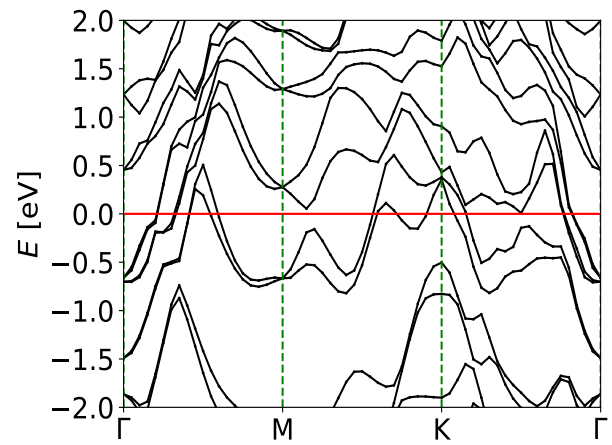
(a) 1 Layer of Pb (111) grown on 1 quintuple layer of Sb_2S_3 substrate



(b) 1 Layer of Pb (111) grown on 1 quintuple layer of Sb_2Se_3 substrate

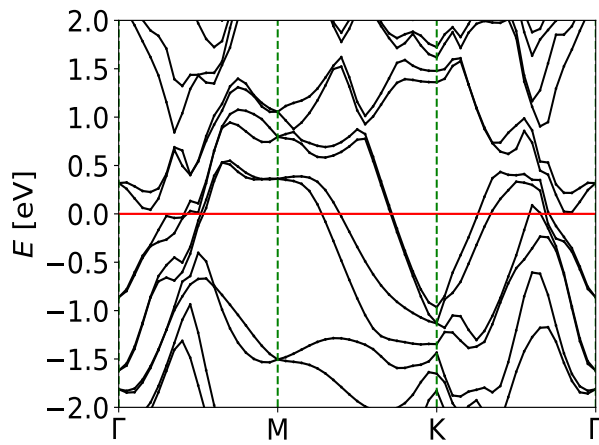


(c) 1 Layer of Pb (111) grown on 1 quintuple layer of Bi_2Se_3 substrate

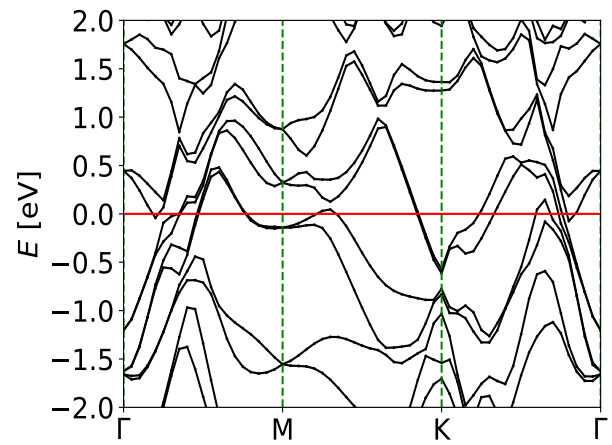


(d) 1 Layer of Pb (111) grown on 1 quintuple layer of Bi_2Te_3 substrate

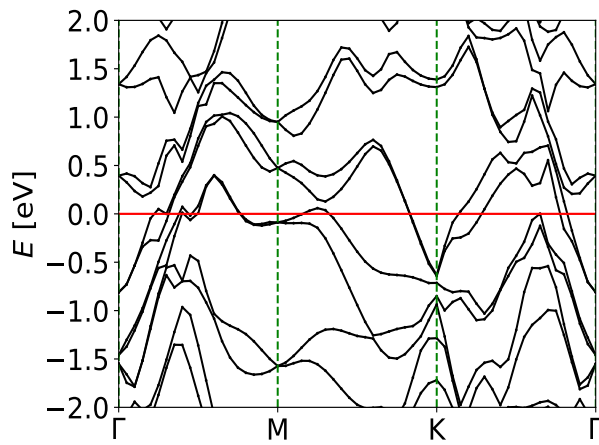
FIG. 24: Band structure of a single layer Pb (111) grown on different substrates



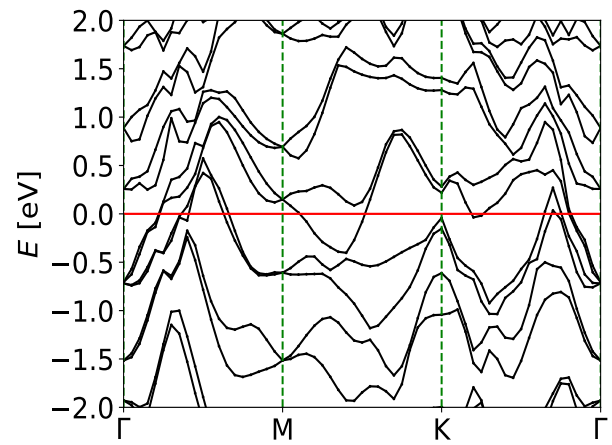
(a) 2 Layer of Pb (111) grown on 1 quintuple layer of Sb_2S_3 substrate



(b) 2 Layer of Pb (111) grown on 1 quintuple layer of Sb_2Se_3 substrate

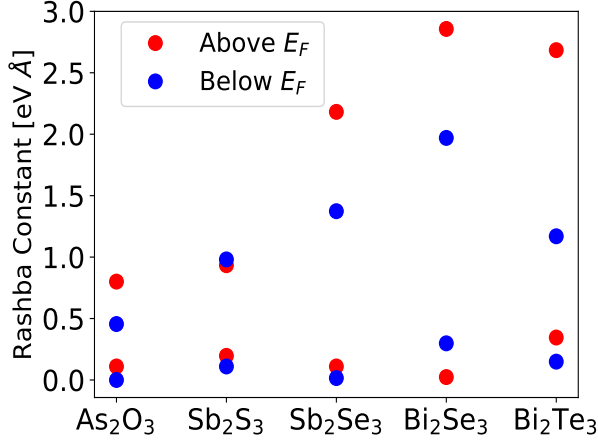


(c) 2 Layer of Pb (111) grown on 1 quintuple layer of Bi_2Se_3 substrate

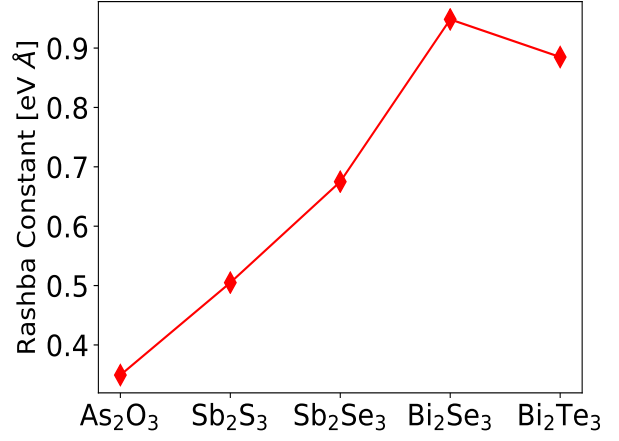


(d) 2 Layer of Pb (111) grown on 1 quintuple layer of Bi_2Te_3 substrate

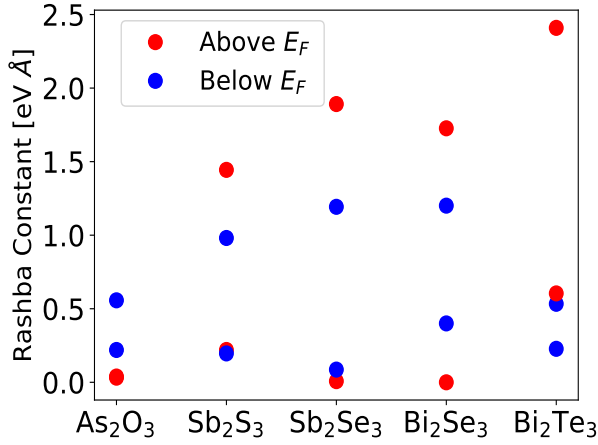
FIG. 25: Band structure of a 2 layers Pb (111) grown on different substates



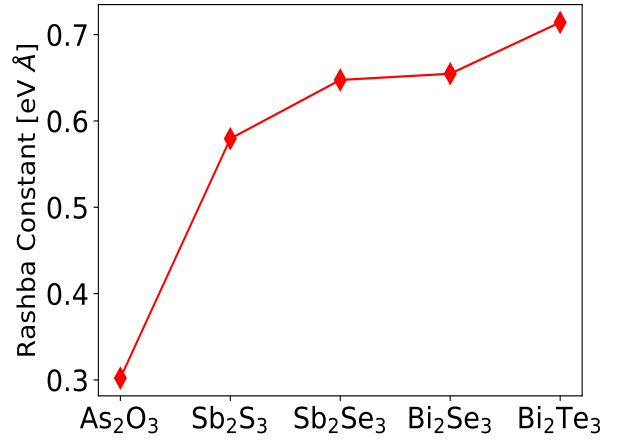
(a) Rashba coupling of 1 layer Pb (111) grown on different substrates



(b) Average Rashba coupling of 1 layer Pb (111) grown on different substrates

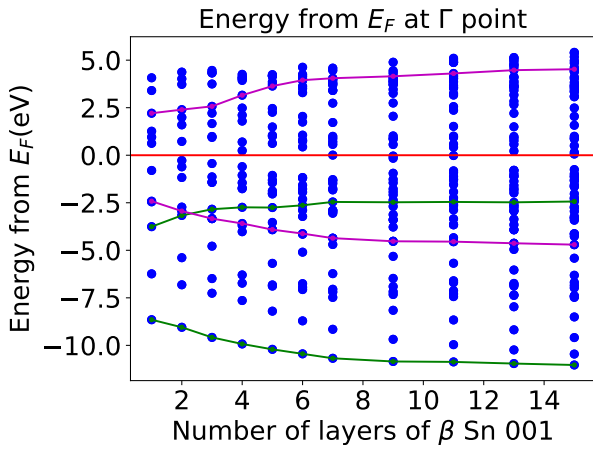


(c) Rashba coupling of 2 layer Pb (111) grown on different substrates

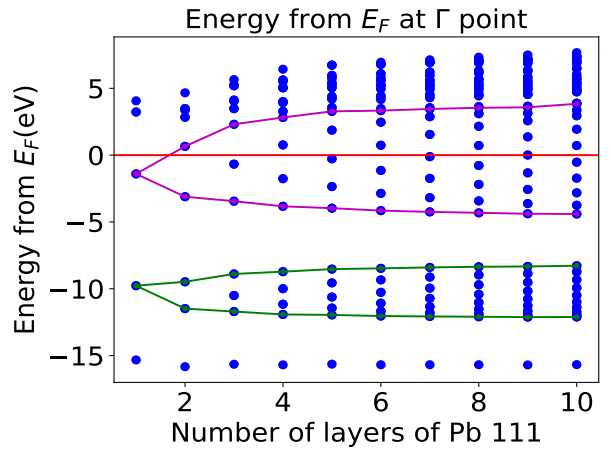


(d) Average Rashba coupling of 2 layer Pb (111) grown on different substrates

FIG. 26: Rashba coupling of a 1 and 2 layers Pb (111) grown on different substates, the average is performed on the 12 subbands around Fermi level, that is 6 above and 6 below.



(a) Energy from Fermi level for Sn (001) thin film



(b) Energy from Fermi level for Pb (111) thin film

FIG. 27: Energy from Fermi level for Sn (001) and Pb (111) thin film

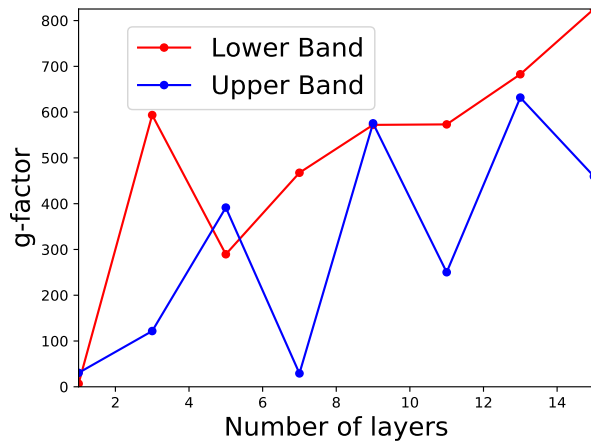
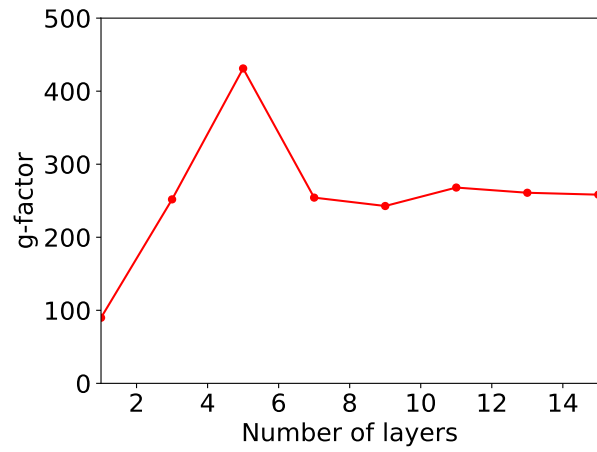
(a) g-factor of the bands around Fermi level at Γ point(b) Average g-factor of the bands around Fermi level at Γ point

FIG. 28: g-factor vs number of layers for Sn (001) thin film

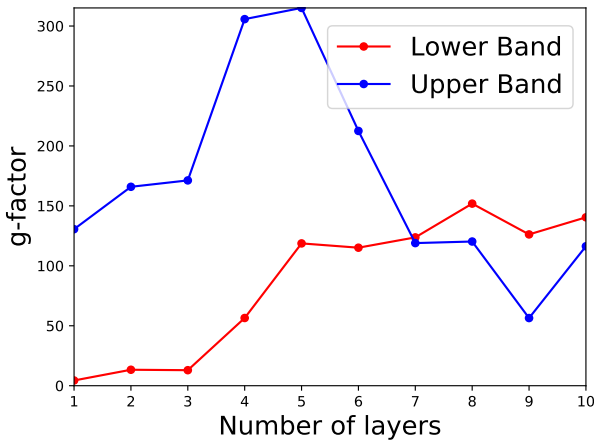
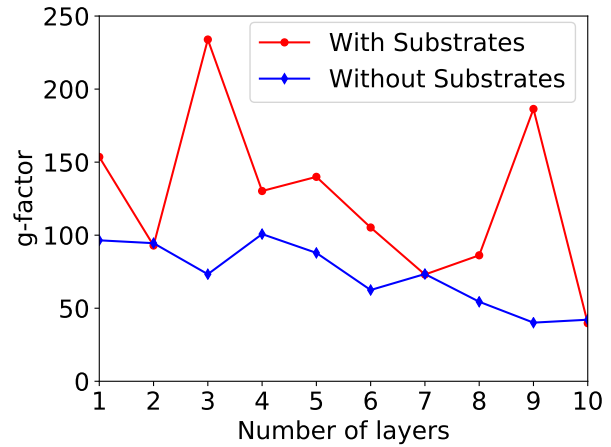
(a) g-factor of the bands around Fermi level at Γ point(b) Average g-factor of the bands around Fermi level at Γ point

FIG. 29: g-factor vs number of layers for Pb (111) thin film